Chapter 4. Nanostructures Technology, Research, and Applications

Academic and Research Staff

Professor Henry I. Smith, Dr. Mark L. Schattenburg, Richard J. Aucoin, James M. Carter, Robert C. Fleming, Euclid E. Moon, Irving Plotnik, Scott E. Silverman

Visiting Scientists and Research Affiliates

Nubuyoshi Koshida[1]

Graduate Students

Martin Burkhardt, David J. Carter, Mike T. Chou, Jay N. Damask, Sean M. Donovan, Juan Ferrera, Nitin Gupta, Scott D. Hector, Hang Hu, James J. Hugunin, Arvind Kumar, Huiying Li, Alberto M. Moel, Akbar A. Moolji, Gabrielle M. Owen, Satyen Shah, Vincent V. Wong, Isabel Y. Yang, Anto Yasaka, Kenneth W. Yee

Undergraduate Students

Julie C. Lew, Brian M. Smith

Technical and Support Staff

Donna R. Martinez, Mark K. Mondol, Jeanne M. Porter, Robert D. Sisson

4.1 NanoStructures Laboratory

The NanoStructures Laboratory (NSL) at MIT (formerly the Submicron Structures Laboratory) develops techniques for fabricating surface structures with feature sizes in the range from nanometers to micrometers and uses these structures in a variety of research projects. The NSL includes facilities for lithography (photo, holographic electron beam, ion beam, and x-ray), etching (chemical, plasma and reactive-ion), liftoff, electroplating, sputter deposition, and e-beam evaporation. Much of the equipment and nearly all of the methods utilized in the NSL are developed in house. Generally, commercial integrated circuit (IC) processing equipment cannot achieve the resolution needed for nanofabrication, and it lacks the required flexibility. Research projects, described briefly below, fall into four major categories: (1) development of submicron and nanometer fabrication technology; (2) nanometer and quantum-effect electronics; (3) periodic structures for x-ray optics; spectroscopy and atomic interferometry; and (4) crystalline films on non-lattice-matching substrates.

4.2 Scanning Electron-Beam Lithography Facility

Sponsors

Joint Services Electronics Program
Contract DAAL03-92-C-0001
Semiconductor Research Corporation
Contract 94-MJ-550

Project Staff

Scott E. Silverman, Professor Henry I. Smith, Juan Ferrera

Since its inception in 1978, the Submicron Structures Laboratory (recently renamed the NanoStructures Laboratory) has relied on outside facilities, most notably the Naval Research Laboratory (NRL) in Washington, D.C., and IBM in Yorktown Heights, New York, for scanning-electron-beam lithography (SEBL). In November 1993 we received, as a donation from IBM, an SEBL system, designated the VS-2A, shown in figure 1.

[1] Tokyo University of Agriculture and Technology, Tokyo, Japan.

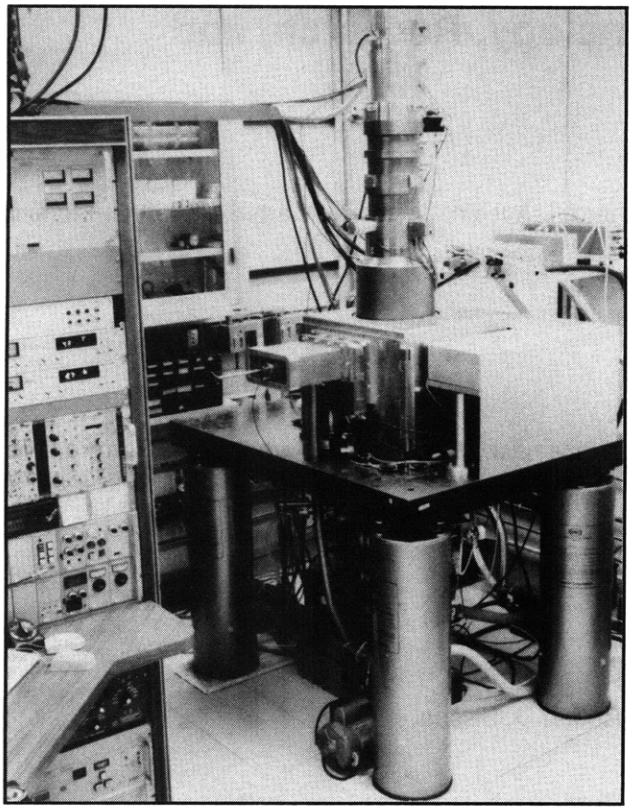

Figure 1. Photograph of VS-2A scanning-electron-beam lithography system donated to MIT by IBM.

This is an experimental system based on many years of IBM technology development in SEBL. The VS-2A system will be the cornerstone of a new SEBL facility located in Building 38. The new facility should be in full operation by May 1994.

The goals of the new facility are to (1) provide the MIT research community with an in-house SEBL capability for writing directly on experimental device substrates; (2) advance the state-of-the-art in SEBL, particularly with regard to pattern placement accuracy and long-range spatial phase coherence; and (3) pattern x-ray nanolithography masks. Our approach to improved pattern placement accuracy is based on a new technique, recently invented at MIT, called spatial-phase locking. It is expected that the new SEBL facility will concentrate on sub-100 nm electronic and quantum-effect devices and optoelectronic devices such as DFB lasers and channel dropping filters for wavelength-division multiplexing in optical communication systems.

4.3 Spatial-Phase-Locked Electron-Beam Lithography

Sponsors

Joint Services Electronics Program
Contract DAAL03-92-C-0001
Semiconductor Research Corporation
Contract 94-MJ-550
U.S. Army Research Office
Grant DAAL03-92-G-0291

Project Staff

James M. Carter, Juan Ferrera, Scott E. Silverman, Professor Henry I. Smith, Vincent V. Wong

It is well known that scanning-electron beam lithography can write extremely fine lines, ~10 nm in thin PMMA and ~1 nm in AlF_3. However, because writing fields in electron-beam lithography are quite small (10^3 to 10^4 beam steps), large-area patterns must be created by stitching together the small fields, using a laser interferometer to provide X-Y positioning information. However, it is often overlooked that, due to instability and drift, the precision with which this can be done is much poorer than the resolution. Typically, stitching errors of 20 to 50 nm (often larger) are observed at field boundaries.

We have proposed to solve this problem by developing a technology we call spatial-phase-locked electron-beam lithography (SPLEBL), which will provide pattern placement accuracy and precision finer than the resolution. A global fiducial grid is placed on the substrate. The grid is created by holographic lithography, ensuring long-range spatial-phase coherence. It is transparent to the beam, but enables a control computer to keep track of the beam location by means of phase-locking techniques and thus correct for any drift in the system.

In order to demonstrate the efficacy of SPLEBL, x-ray masks for distributed-feedback lasers and channel-dropping filters were fabricated in collaboration with IBM's Thomas J. Watson Research Center. These classes of devices have linewidths of ~115 nm and span many fields of the e-beam lithography system. They require field stitching errors of ~1 nm for good performance. We have achieved stitching errors below 2 nm and have demonstrated sub-nanometer repeatability for spatial-phase locking. Initial results are shown in figures 2 through 4.

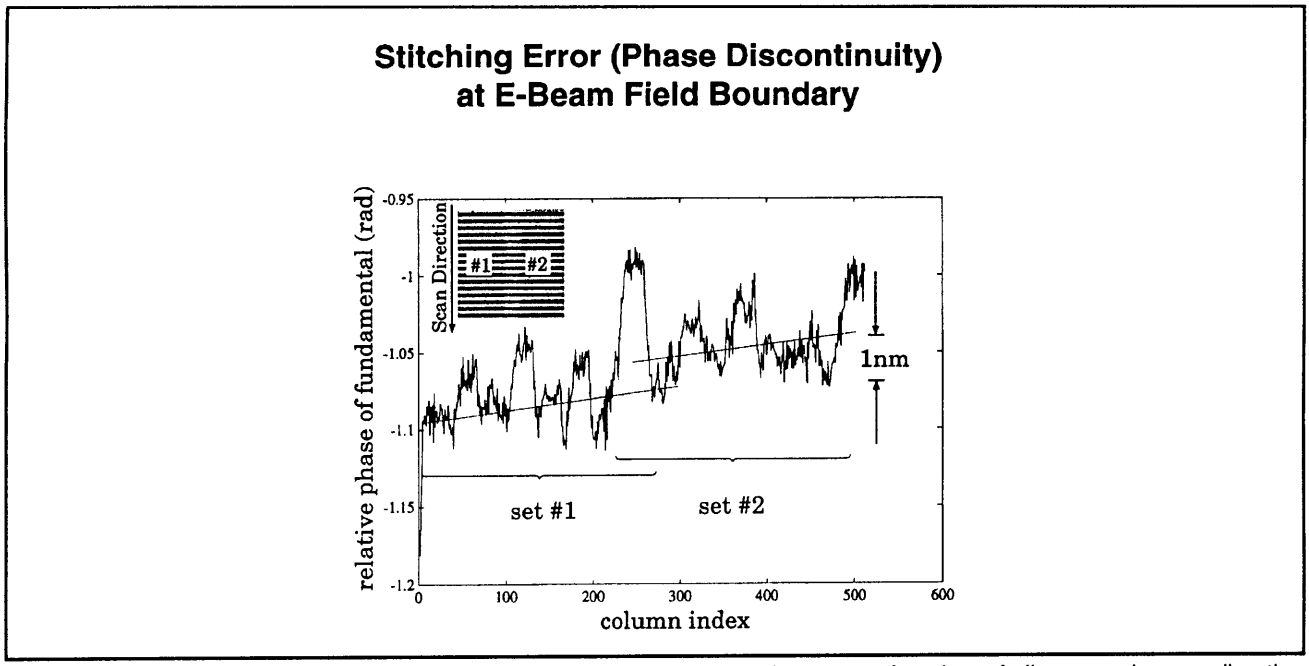

Figure 2. Measurement of the spatial-phase of two overlapped gratings as a function of distance along a direction parallel to the grating lines, as depicted in inset. Set 1 was written using a fiducial grating as a guide. Then the stage was moved and set 2 written, again using the fiducial grating as a guide. Stitching error is below the noise level (i.e., <2 nm).

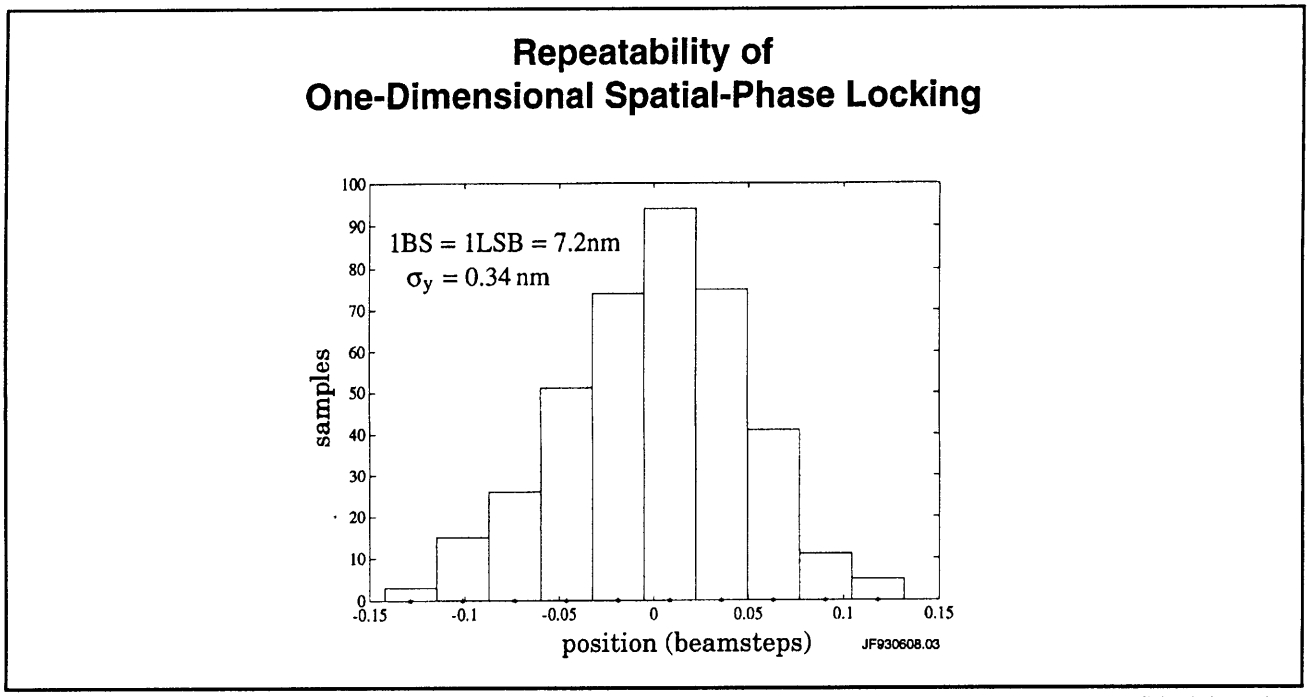

Figure 3. Histogram of the phase difference between two successive frame acquisitions on a reference fiducial grating, corrected for stage drift. The standard deviation value of 0.3 nm represents the repeatability or precision of spatial-phase locking in 1-D for our experimental conditions: 8 periods of the 200 nm gold reference grating per viewing window; 100 pA beam current at 50 kV; a p-n diode backscatter detector.

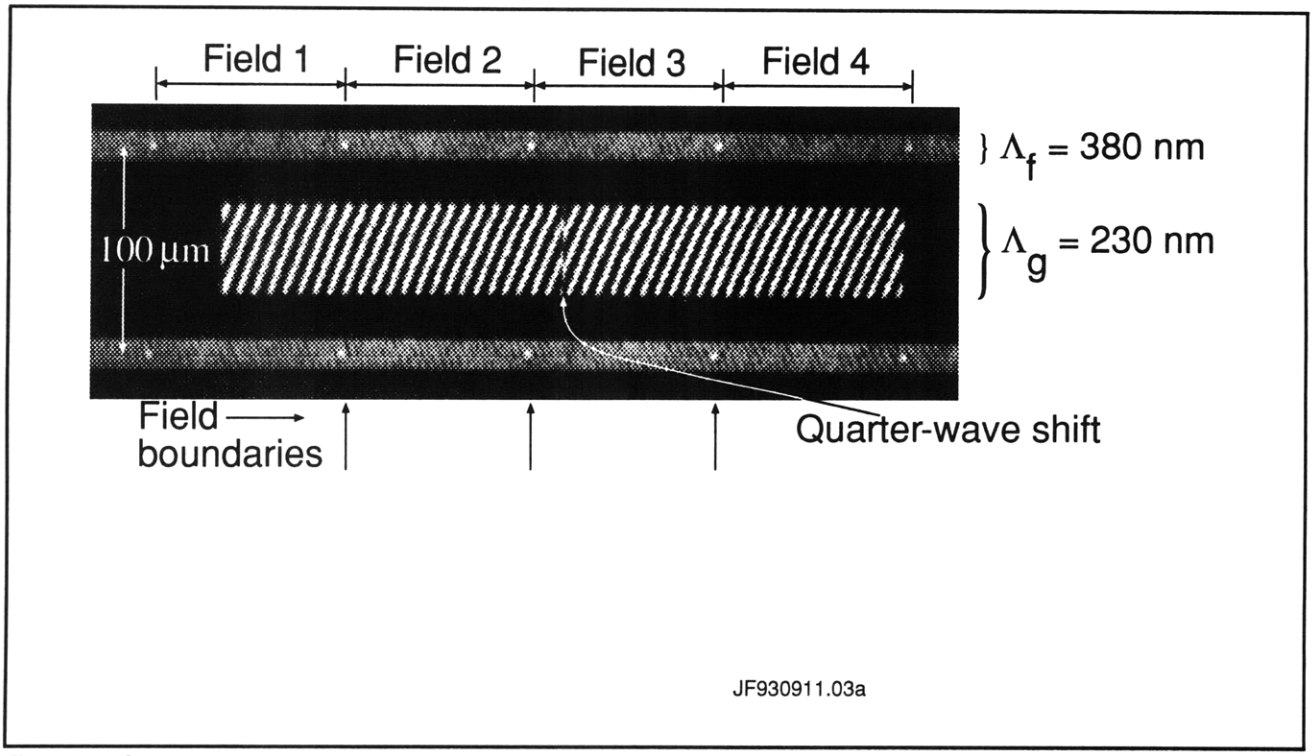

Figure 4. Scanning-electron micrograph of a channel-dropping filter (CDF) grating (spatial period 230 nm) written across four scan fields of the e-beam lithography system. The gratings, which are too fine to be seen directly, are made visible via a moiré between them and the SEM scan raster. The fiducial reference (spatial period = 380 nm) was put in the substrate in advance. The quarter-wave phase step is clearly visible in the CDF grating, but no phase errors are visible at the boundaries of the four scan fields.

4.4 X-Ray Nanolithography

Sponsors

Advanced Research Projects Agency/
Naval Air Systems Command
Contract N00019-92-K-0021
Joint Services Electronics Program
Contract DAAL03-92-C-0001
National Science Foundation
Grant ECS 90-16437

Project Staff

James M. Carter, Nitin Gupta, Scott D. Hector, Gabrielle M. Owen, Dr. Mark L. Schattenburg, Professor Henry I. Smith, Vincent V. Wong, Isabel Y. Yang

For several years, we have been developing the tools and methods of x-ray nanolithography (i.e., sub-100 nm features). We have explored its theoretical and practical limitations, and endeavored to make its various components (e.g., mask making, resists, electroplating, sources, alignment, etc.) reliable and "user friendly". Because of the critical importance of the x-ray mask technology, we discuss this in a separate section (4.5).

Our sources for x-ray nanolithography are simple, low-cost electron-bombardment targets, typically Cu_L (λ = 1.32 nm), separated by a 1.4 μm-thick SiN_x vacuum windows from helium-filled exposure chambers. In the future we hope to replace the Cu_L sources with higher flux plasma-based x-ray sources.

For most applications that require multiple mask alignment, we currently use a simple microscope-based system which provides about 0.3 μm superposition precision. We are also developing (see section 4.6) a high precision mask alignment system that should provide overlay approaching 1 nm.

In earlier research, we showed that for x-ray wavelengths longer than ~0.8 nm, the range of the photoelectron emitted when an x-ray photon is absorbed in resist does not limit the resolution. Down to feature sizes ~20 nm, diffraction is the major concern. By means of accurate electromagnetic calculations, taking into account the vectorial character of the electromagnetic field and the dielectric properties of the absorber, we have shown that when source spatial coherence is optimized, diffraction does not limit resolution as

severely as had been predicted by simple Fresnel diffraction calculations.

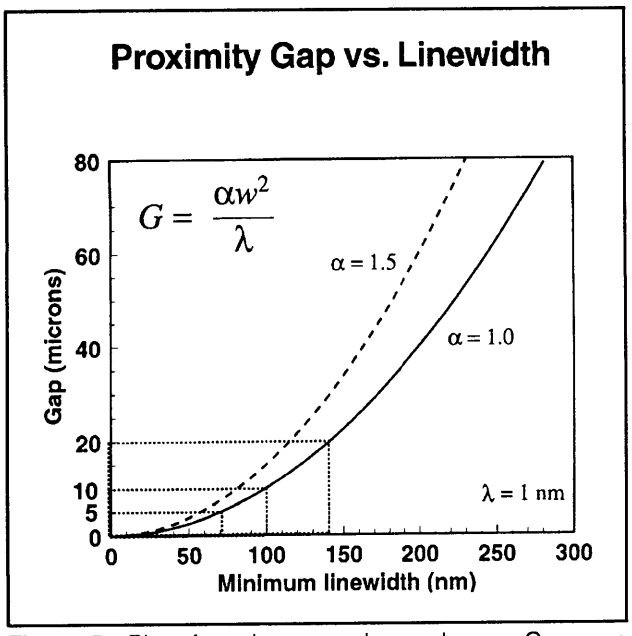

Figure 5. Plot of maximum mask-sample gap, G, versus minimum feature size, W, for two values of the parameter α.

Figure 5 plots the maximum mask-to-sample gap, G, versus minimum feature size, W, for two values of the parameter α which connects gap and feature size: $G = \alpha W^2/\lambda$. Modeling and experiment verify that α can be as large as 1.5 while retaining good process latitude.

For the linewidth range from 70 to 20 nm, mask-substrate gaps must be below 5 μm. This is not a problem in research but for manufacturing may be unacceptable. For this reason, we investigated the feasibility of using arrays of zone plates for projection imaging with x-rays of either 4.5 nm or ~1.0 nm wavelength.

4.5 Improved Mask Technology for X-Ray Lithography

Sponsors

Advanced Research Projects Agency/
Naval Air Systems Command
Contract N00019-92-K-0021
Joint Services Electronics Program
Contract DAAL03-92-C-0001
National Science Foundation
Grant ECS 90-16437

Project Staff

Martin Burkhardt, James M. Carter, Juan Ferrera, Scott D. Hector, Huiying Li, Mark K. Mondol, Gabrielle M. Owen, Dr. Mark L. Schattenburg, Robert D. Sisson, Professor Henry I. Smith, Vincent V. Wong, Isabel Y. Yang

At feature sizes of 100 nm and below, the mask-to-sample gap, G, must be less than ~10 μm. We have developed a mask configuration compatible with this requirement in which the mask membrane is flat to < 250 nm. We continue to make incremental improvements in this technology aiming at a process that will enable x-ray mask blanks to be fabricated almost entirely with automated IC processing equipment.

Our mask technology is based on low-stress, Si-rich silicon nitride, SiN_x. This material is produced in the IC Laboratory at MIT in a vertical LPCVD reactor. The resulting films are clean and uniform, and x-ray mask membranes made from them are extremely robust. They can be cleaned and processed in conventional stations. Radiation hardness remains a problem at dose levels corresponding to production (i.e., millions of exposures) but for research the material is quite suitable.

For absorber patterns we use both gold, Au, and tungsten, W. Both can be obtained with near-zero stress (i.e., < 10^7 MPa) which implies that pattern distortion should be negligible (i.e., < 1 nm). The gold is electroplated onto the membrane after resist exposure and development using a specially designed apparatus. The W is sputter deposited and patterned by reactive-ion etching. During sputter deposition, the plasma environment leads to a nonuniform temperature distribution, which, in turn, causes nonuniform stress. In order to ensure uniform W stress over an entire membrane, a He-backside temperature homogenization apparatus was constructed. Heat is transferred to the membrane from a heated aluminum block separated from the membrane by a 1 mm gap. Results are shown in figure 6. We verify the achievement of stress < 10^7 MPa using a Linnik interferometer equipped with a CCD, a frame grabber and special purpose software that averages out-of-plane deflection over an entire frame.

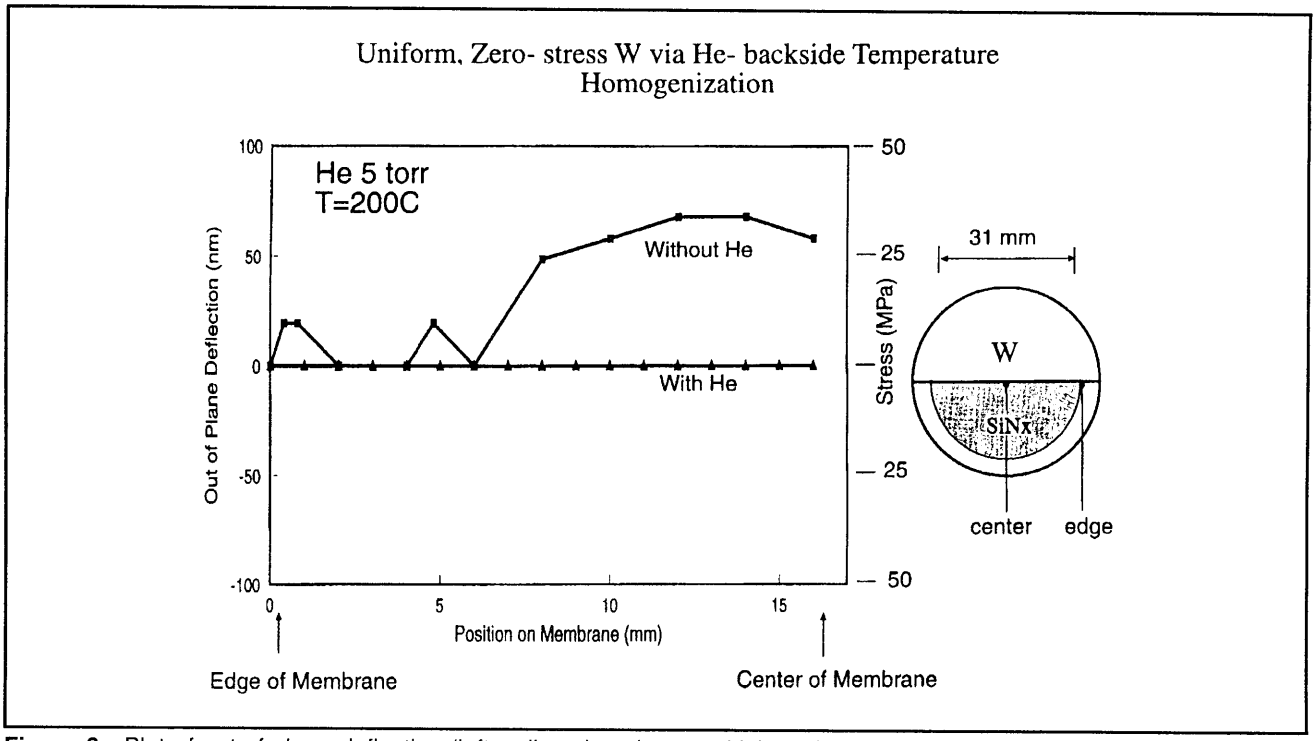

Figure 6. Plot of out-of-plane deflection (left ordinate) and stress (right ordinate) versus radial position for 300 nm-thick W, sputter deposited at 200°C onto a SiN_x x-ray mask membrane, with and without He backside temperature homogenization. A uniform zero stress is achieved with He, whereas stress is nonuniform without the He.

We have also constructed an apparatus that makes precision measurements of membrane deflection in response to gas pressure differential. This "bulge tester" will enable us to make non-destructive measurements of absorber stress in the low 10^6 MPa range.

Patterning of x-ray masks is done by holographic lithography for periodic structures but, for patterns of arbitrary geometry, it is done by e-beam lithography, either in the MIT e-beam facility or in collaboration with NRL or IBM. We use CAD tools at MIT and convert the data into formats compatible with the e-beam exposure systems. Data is shipped to NRL or IBM by electronic mail. After e-beam exposure, masks are shipped back to MIT by express mail where development and Au electroplating are carried out. This collaboration has already demonstrated that patterning x-ray masks by e-beam can be done remotely, and, by implication, that university researchers with limited facilities can have access to nanolithography via x-ray alone and do not need to own or even visit an e-beam lithography facility. Figure 7 shows an x-ray mask of a coulomb-blockade device in which the finest linewidth in the 200 nm-thick electroplated gold is 40 nm.

For patterning x-ray masks with W absorber, a reactive-ion-etching process is required which puts considerable power into the membrane substrate. Since membranes have very low thermal mass and conductivity, we use He- backside cooling in a reactive ion etcher. Membranes can be cooled to below -20°C. At such low temperatures the isotropic etching component is suppressed leading to highly directional etching.

4.6 A High Precision Mask Alignment System

Sponsors

Advanced Research Projects Agency/
Naval Air Systems Command
Contract N00019-92-K-0021
Joint Services Electronics Program
Contract DAAL03-92-C-0001

Project Staff

Euclid E. Moon, Professor Henry I. Smith

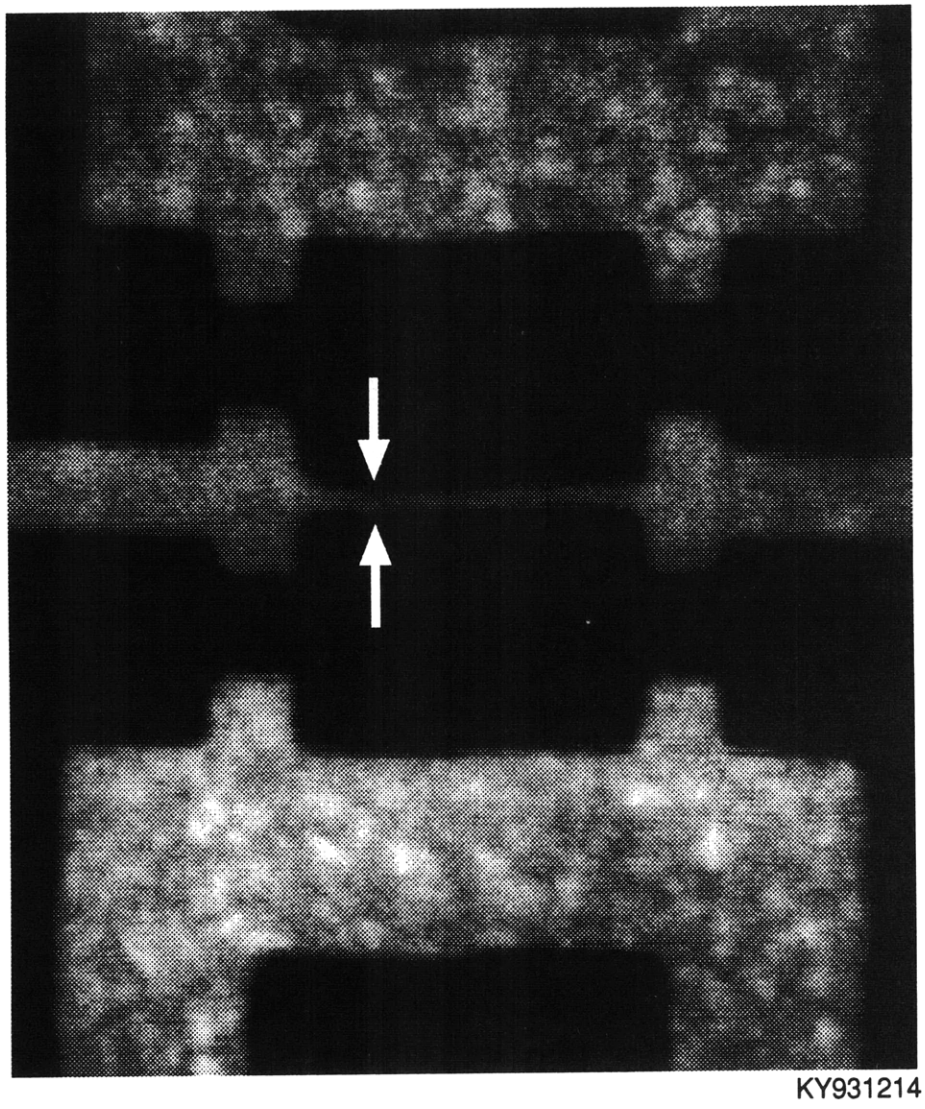

Figure 7. Scanning-electron micrograph of an x-ray mask of a coulomb-blockade device (so-called "single-electron transistor") in which the tunnel-barrier gate is only 40 nm wide. The mask pattern was written by scanning-electron-beam lithography at the Naval Research Laboratory, and the electroplating to 200 nm thickness was done at MIT.

In order for any lithographic technique to be of general utility, a compatible alignment technique must also be provided. The technique must be capable of superposition precision that is a small fraction of the minimum feature size. Previously, we demonstrated a new scheme for aligning x-ray masks to substrates that was based on the principle of on-axis interference from gratings on the mask and substrate that differ in spatial period (e.g., p_1 on mask, p_2 on the substrate). The interference pattern was compared in spatial phase to a fixed fiducial on the mask using a CCD camera and frequency domain image analysis. An alignment standard deviation of 6 nm was achieved. The goal of the present work is threefold: first, to improve the superposition precision by an order of magnitude; second, to fully automate the alignment process; and third, to make the system compatible with industrial x-ray lithography sources and steppers. In order to improve the superposition precision, a new alignment mark was designed that consists of two adjacent gratings on the mask (p_1 and p_2) facing two complementary gratings on the substrate (p_2 and p_1). The resulting on-axis interference pattern consists of two sets of fringes of the same spatial period which move in opposite directions.

By matching them in spatial phase, one achieves alignment. We believe that in conjunction with a CCD and appropriate image processing, a superposition precision below 1 nm can be achieved. Figure 8 illustrates the basic principle.

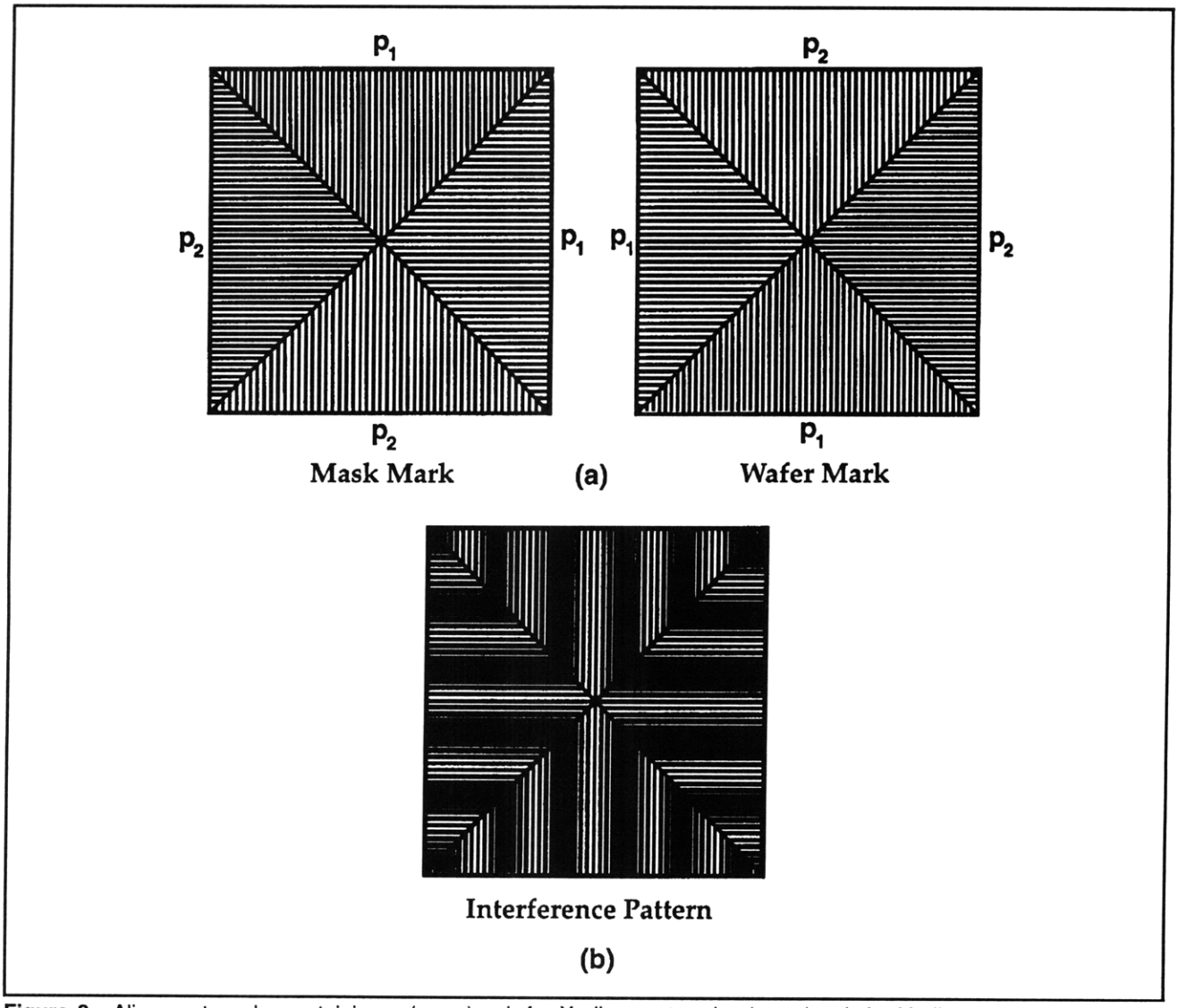

Figure 8. Alignment marks containing a (p_1, p_2) pair for X alignment and a (p_1, p_2) pair for Y alignment. (a) Marks for mask and substrate. (b) Depiction of interference pattern that would be obtained when mask and substrate are aligned in both X and Y.

A new X, Y, Z, θ stage is being constructed which incorporates high-resolution closed-loop drives and piezos with sub-nanometer repeatability. A wide variety of masks and wafers can be accommodated, including the NIST and MIT mask standards, as well as small substrates and eight inch wafers. An automatic image acquisition and alignment algorithm has been written which compares the spatial-phases of an on-axis interference pattern in about 200 msec. These improvements will be incorporated in a system configuration, shown in figure 9, which is consistent with those under development in industry.

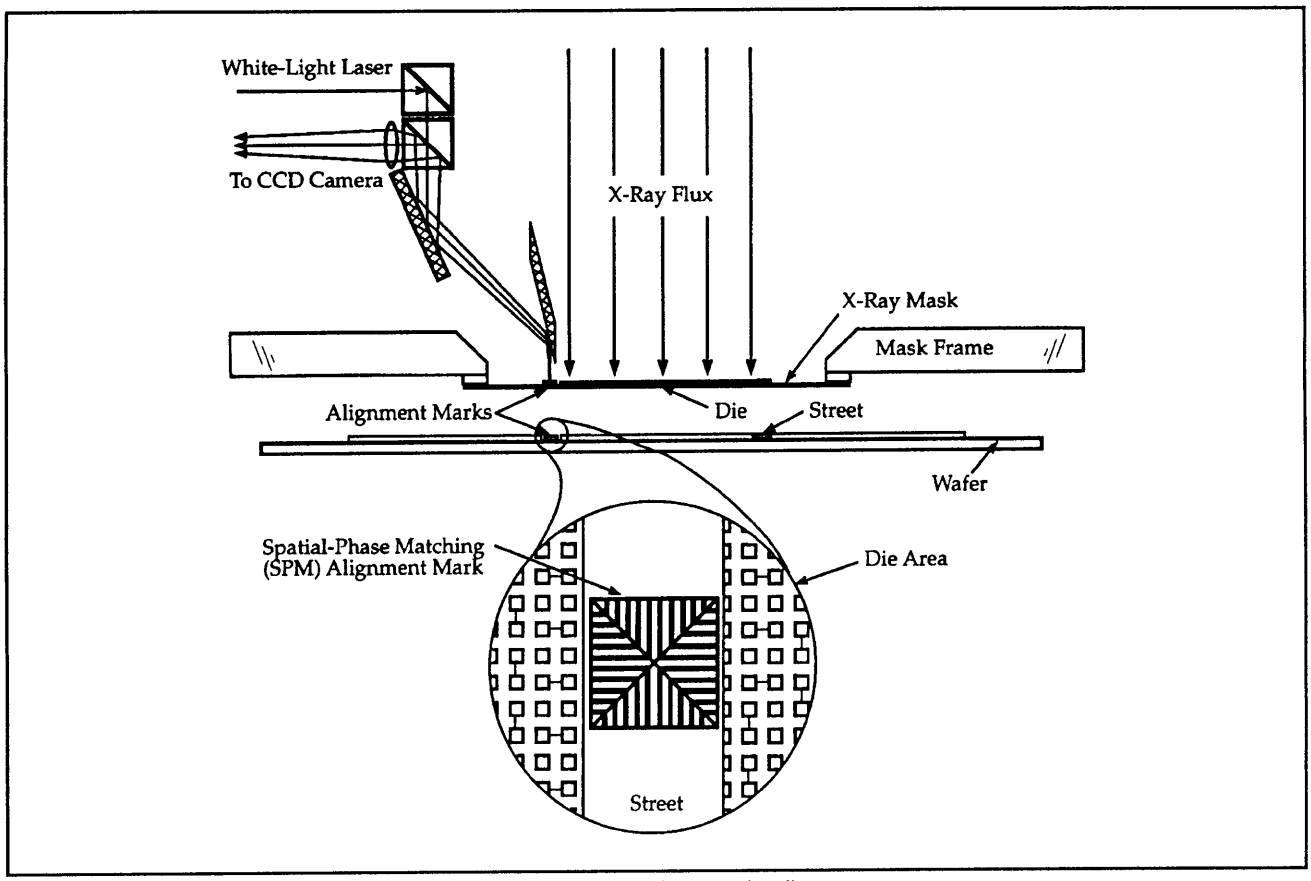

Figure 9. Schematic of optical configuration for on-axis interferometric alignment system.

4.7 Optimization of Synchrotron-Based X-ray Lithography

Sponsors

Advanced Research Projects Agency/
Naval Air Systems Command
Contract N00019-92-K-0021
National Science Foundation
Grant ECS 90-16737

Project Staff

Richard J. Aucoin, Scott D. Hector, Dr. Mark L. Schattenburg, Professor Henry I. Smith

There are two approaches to high flux x-ray sources for commercial x-ray lithography: hot, dense plasmas, generated either by lasers or electrical discharges; and synchrotrons. Traditionally, the former have operated around λ = 1.4 nm and the latter below λ = 1 nm, with a substantial fraction of the absorbed power below the Si K edge at 0.7 nm. Operation at the shorter wavelengths dictates thicker absorber (~0.6 μm) which becomes a difficult task at 100 nm linewidths. Our analysis indicates that the peak of the synchrotron spectrum absorbed by resist can be shifted to 1 nm or even longer without loss of exposure efficiency. This is illustrated in figure 10. Such a shift would greatly simplify the mask-making task. However, to accomplish this the 25 μm-thick Be vacuum window currently used in synchrotrons must be replaced by a ~2 μm-thick Si window. We have demonstrated that SiN_x membranes this thick can withstand a pressure differential of one atmosphere. We are currently testing various versions of elliptical (2.5 x 55 nm) windows as possible vacuum windows for synchrotrons.

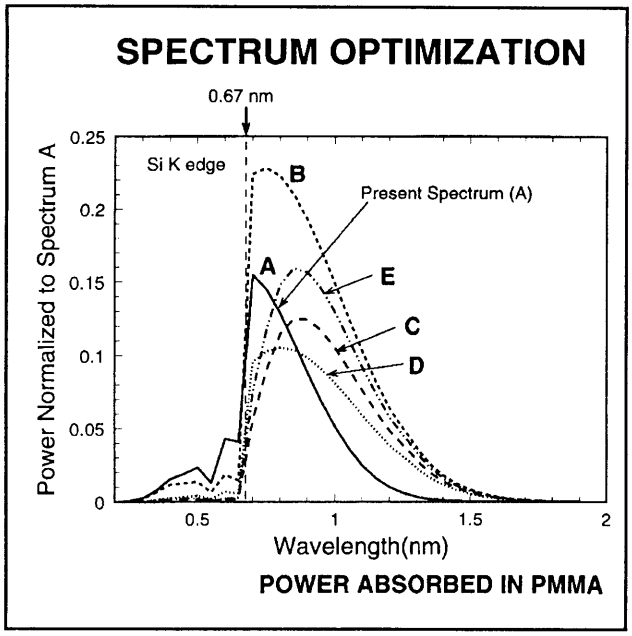

Figure 10. Comparison of the current Helios synchrotron spectrum (A) with four alternative spectra achieved by use of a 2 μm-thick Si vacuum window and modification of either the beam energy or the beam-line mirror angle. By shifting the peak to longer wavelength, spectra B, C, D, and E require thinner mask absorber and increase the x-ray power absorbed in the resist. Spectrum E is preferred.

4.8 Achromatic Holographic Lithography

Sponsor

Joint Services Electronics Program
Contract DAAL03-92-C-0001

Project Staff

James M. Carter, Satyen Shah, Professor Henry I. Smith

Holographic schemes are preferred for the fabrication of periodic and quasi-periodic patterns that must be spatially coherent over large areas, and free of phase steps. For spatial periods below 200 nm, light sources with wavelengths below 200 nm must be used. All such sources have limited temporal coherence, and thus one is forced to employ an achromatic scheme, such as shown in figure 11. In order to make the apparatus more reliable, the depth-of-focus had to be increased. To this end, we introduced a collimating lens and a slit scanning system. We have also incorporated a white-light interferometer that utilizes optical paths through the quartz plates that closely approximate the paths of the exposing beams. A photodetector and lock-in amplifier (figure 12) are used to find the optimum sample position. With the substrate to be exposed in place, the white light interferometer ensures maximum fringe contrast during exposure with the 193 nm deep-UV radiation. Using these improvements, we can reliably expose 100 nm-period gratings over areas of more than 2 cm^2. We plan to use this system to fabricate 100 nm-period x-ray masks and free-standing gratings for He atom interferometry. We also plan to take the technique one step further to 50 nm periods (25 nm lines and spaces) using a 13 nm undulator as a source.

4.9 Ion Beam Lithography

Sponsor

Joint Services Electronics Program
Contract DAAL03-92-C-0001

Project Staff

Scott E. Silverman, Professor Henry I. Smith, Anto Yasaka

Focused-ion-beam (FIB) systems are potentially useful as nanolithography tools because of the near absence of backscattering, which is a significant problem in electron-beam lithography, especially on high-atomic-number substrates. We currently work with Be^{++} ions and have demonstrated 50 nm lines and spaces. The FIB system is being modified to accept an improved Be alloy source. We will explore the feasibility of combining spatial-phase-locking with FIB lithography. This could prove to be the superior technology for making x-ray nanolithography masks based on W absorbers.

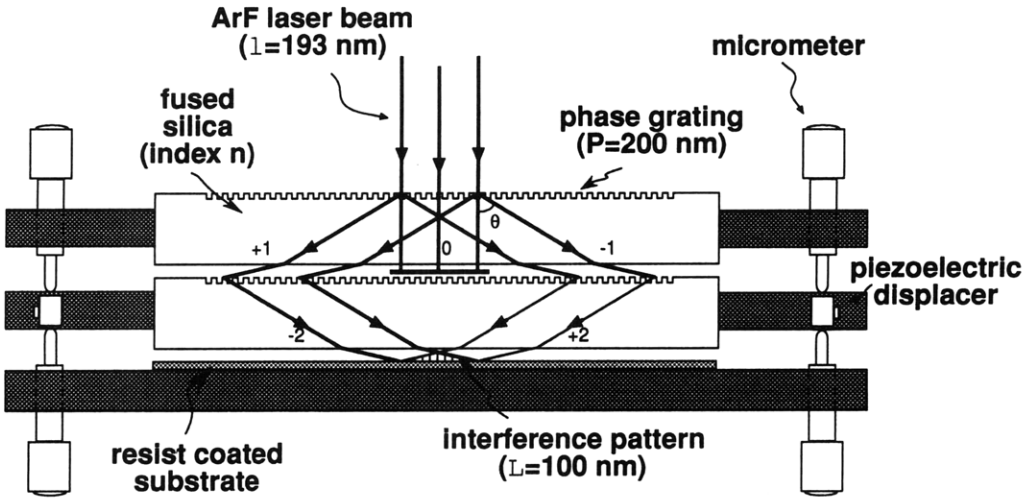

$$\sin\theta = \lambda/(nP),$$

$$\Lambda = \lambda/(2n \sin\theta)$$

$$\Lambda = P/2$$

Figure 11. Achromatic-holographic lithography (AHL) configuration in which the separation between the substrate and the second phase grating is controlled by a piezoelectric micrometer.

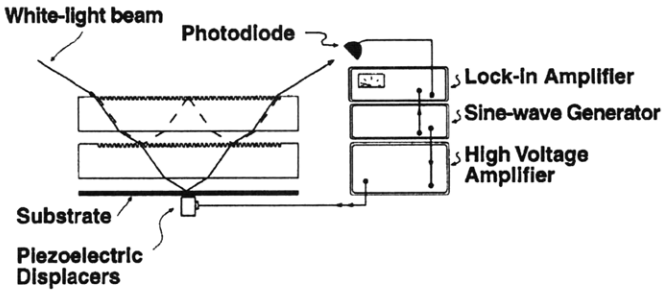

Figure 12. Schematic of white-light interferometer used to match optical path lengths in the AHL configuration. A collimated white-light beam is split into two paths and recombined to interfere at a photodiode. An interference peak, detected via a lock in amplifier, indicates a matching of path lengths and hence maximum image contrast in the AHL configuration.

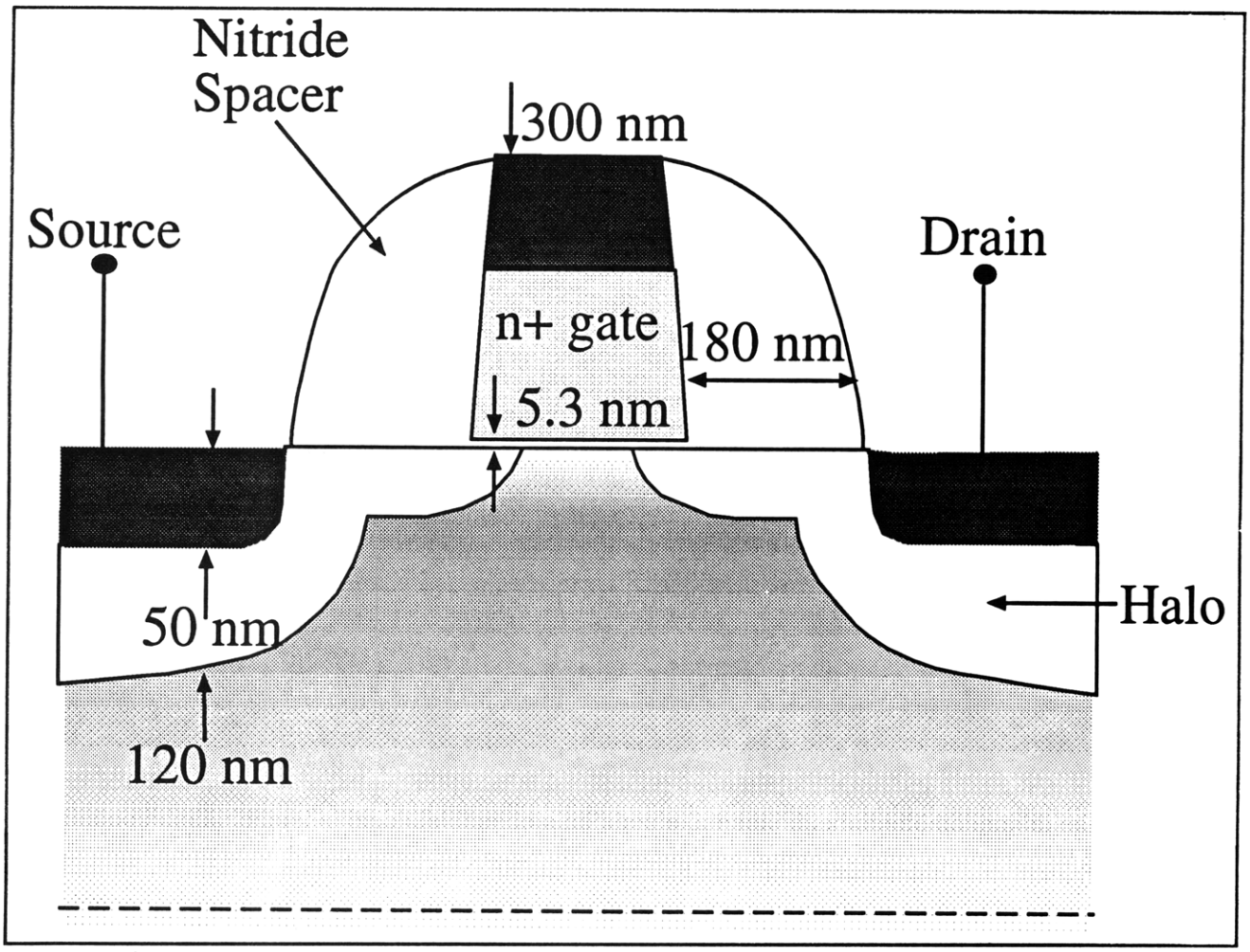

Figure 13. Schematic of 0.1 μm channel-length self-aligned NMOSFET.

4.10 High Performance Self-aligned Sub-100 nm MOSFETs Using X-ray Lithography

Sponsors

Advanced Research Projects Agency/
Naval Air Systems Command
Contract N00019-92-K-0021
IBM Corporation
Contract 1622
Joint Services Electronics Program
Contract DAAL03-92-C-0001

Project Staff

Professor Dimitri A. Antoniadis, James M. Carter, William Chu,[2] Hang Hu, Kee Rhee,[2] Professor Henry I. Smith, Lisa T.-F. Su, Isabel Y. Yang

We have fabricated sub-0.1 μm N-channel MOSFET devices using x-ray lithography. Extremely well-controlled short-channel effects were achieved through appropriate channel and source/drain engineering.

Figure 13 shows the device schematic. The retrograde channel doping profile was accomplished using shallow indium and deep boron implants. The source/drain halo extensions were formed using a low energy arsenic implant with indium pre-amorphization and counter-doping. The self-aligned polysilicon gates were fabricated using x-ray nanolithography and an anisotropic etching process. The aligned, microgap x-ray exposures were carried out using mesa-etched SiN_x x-ray masks with Au absorber pattern. The original (mother) mask patterns were written at the NRL by e-beam lithog-

[2] Naval Research Laboratory, Washington, DC.

raphy, and then several duplicates (daughters) were made using x-ray lithography. We have characterized the chemically amplified resist SAL-601 and developed a process which allowed us to achieve the minimum linewidths with control and a large process latitude. This involved optimization of the post exposure bake time and temperature. We found that with a post-exposure temperature of 110°C and a post-exposure baking time of 40 seconds, minimum linewidths of approximately 100 nm were obtained. To eliminate "skin" formation on top of the SAL-601, a thin (200-250 nm) layer of polyvinyl alcohol (PVA, which is water soluble) was spun on top of the resist. The resist served as a mask for etching a thin LTO layer which, in turn, acted as a hard mask for the selective anisotropic etching of polysilicon using $C1_2$ plasma. Figure 14 shows the self-aligned SAL-601/LTO. Figure 15 shows a polysilicon gate defined by x-ray lithography and $C1_2$ plasma etching.

Figure 16 shows the I-V characteristics of a sub-0.1μm nMOSFET with L_{eff} of 850 nm and 5.3 nm gate oxide. This device has a current drive of 0.74 nA/μm and a saturated transconductance of 500 nS/mm at 2.0 V power supply with a threshold voltage of 0.36 V and a sub-threshold slope of 88.1 mV/dec. This indicates that these 0.1μm MOSFET devices fabricated by x-ray lithography exceed the performance of the current state-of-the-art 0.1μm MOSFET devices produced by e-beam lithography.

4.11 Fabrication of T-gate Devices Using X-ray Lithography

Sponsor

Advanced Research Projects Agency/
Naval Air Systems Command
Contract N00019-92-K-0021

Project Staff

James M. Carter, Nitin Gupta, Professor Henry I. Smith

Monolithic microwave integrated circuits (MMICs) have potential applications in automobile navigation, collision-avoidance, and personal wireless communication systems. High-speed MODFET devices require very short gate lengths, while preserving low resistance. Large gate widths are required for high current drive. To meet these conflicting demands, researchers have developed so-called "T-gate" and "gamma-gate" processes in which the base of the gate is very short (~100 nm) while the upper part is large and overlaps the short base, similar to a mushroom, or the letters T or G. Such structures are readily achieved using direct-write electron-beam lithography (EBL). However, this technology is expensive, slow, and unlikely to meet future production volume needs. For these reasons, we developed a process for fabricating T-gates using x-ray lithography. Initial results were obtained using tri-layer PMMA. The three layers consisted of a bottom one of 950K PMMA, a middle layer of PMMA/MAA (the co-polymer of PMMA), and an upper layer of 496K PMMA. These three resists have different x-ray sensitivities. Experimental results are shown in figures 17 and 18.

Figure 14. Patterning for MOSFET gate with x-ray lithography exposure of chemically-amplified resist SAL-601 and RIE of low-temperature oxide using CHF_3.

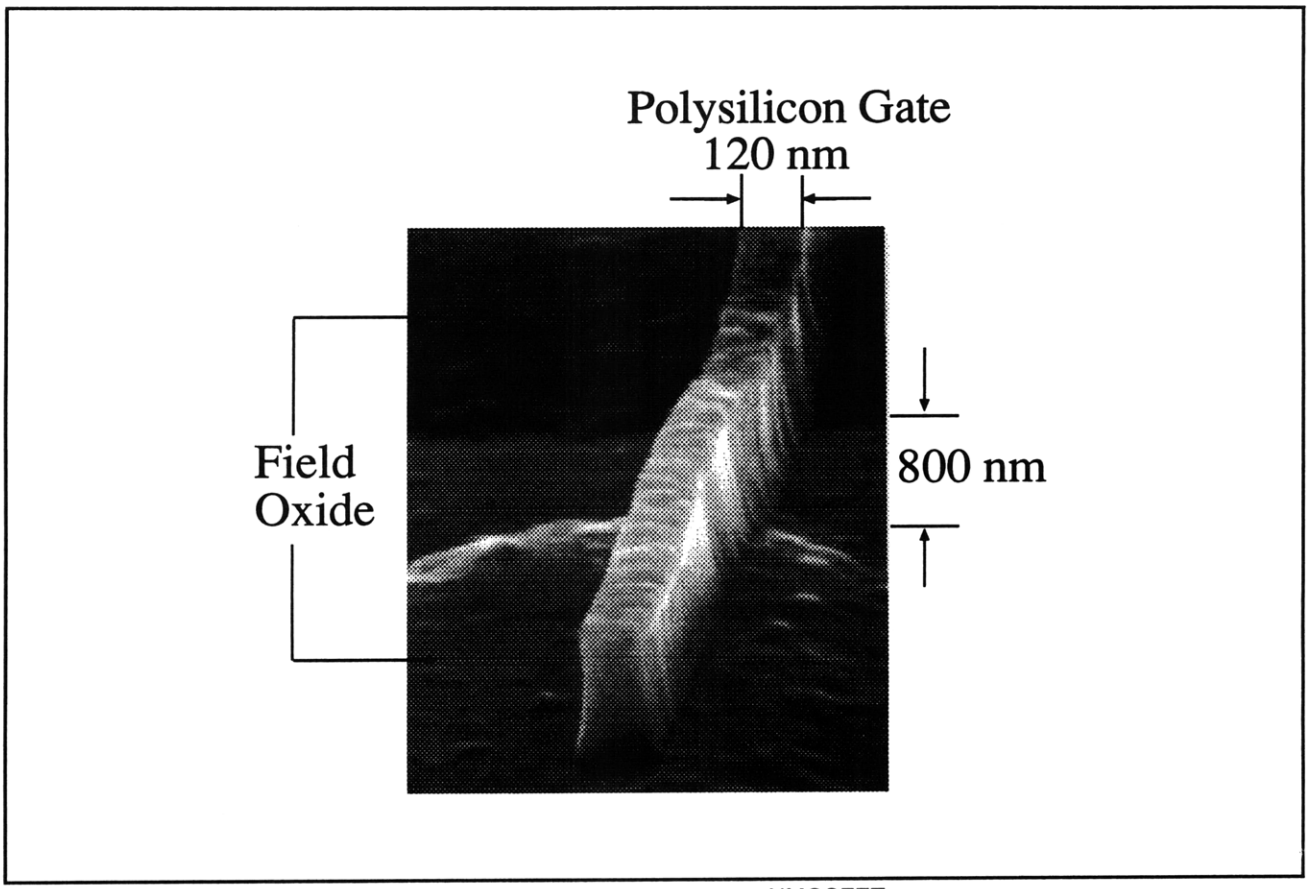

Figure 15. Scanning-electron micrograph of high performance 0.1 μm NMOSFET.

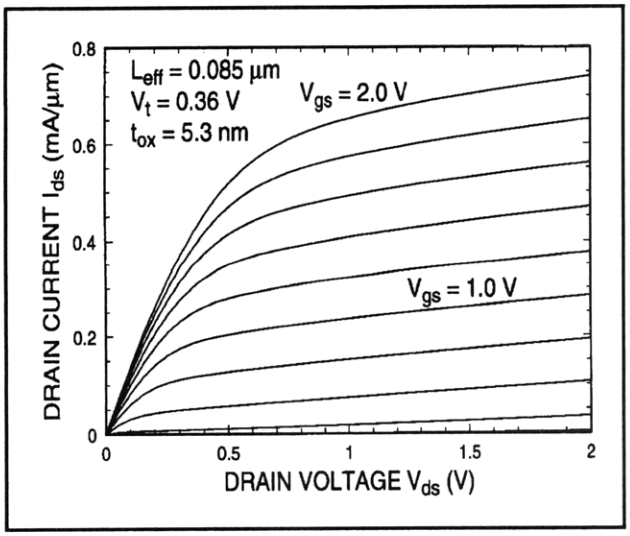

Figure 16. I-V characteristics of a 85 nm-channel-length NMOSFET. The saturated G_m is 500 mS/mm.

Only one alignment, one exposure, and one development are required. However, the process latitude is narrow, and the process may not be suitable for manufacturing.

In order to enhance the process latitude, we are pursuing a bi-layer process that utilizes high-sensitivity chemically amplified resists. This process has the flexibility that arises from two separate alignments, exposures, and developments.

There are a number of interesting directions that may be followed once a high latitude process is established. For manufacturable MMIC systems, both MESFETs and HEMTs are required for low-noise and power applications. Initially, relatively simple GaAs MESFETs will be studied, followed by GaAs and InP HEMTs of varying degrees of complexity. Further studies could include low-temperature-grown GaAs MESFETs for high breakdown voltages, self-aligned devices, or gate materials other than Au, such as W.

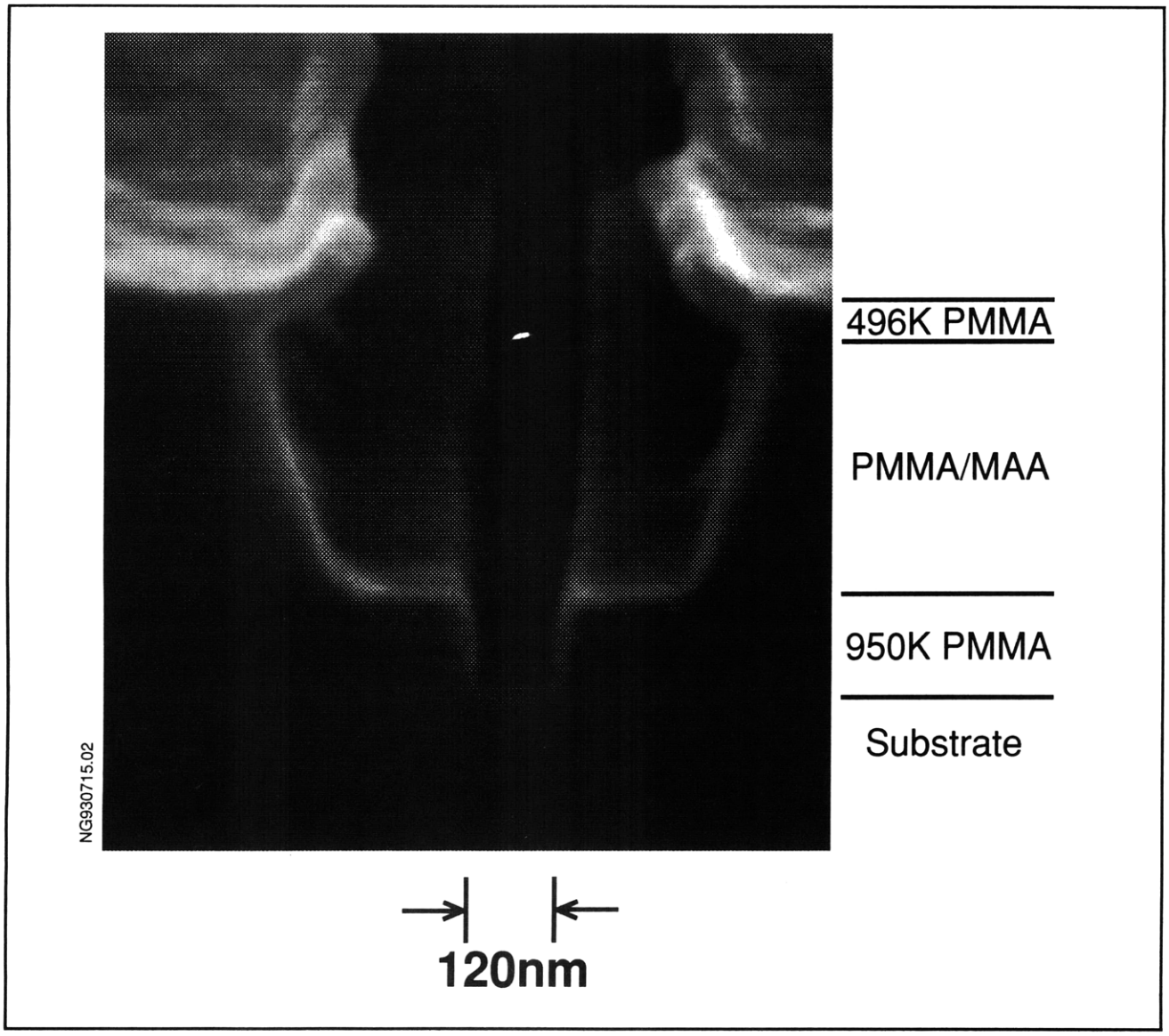

Figure 17. Scanning electron micrograph showing the resist profile cross-section for a 120 nm T-gate.

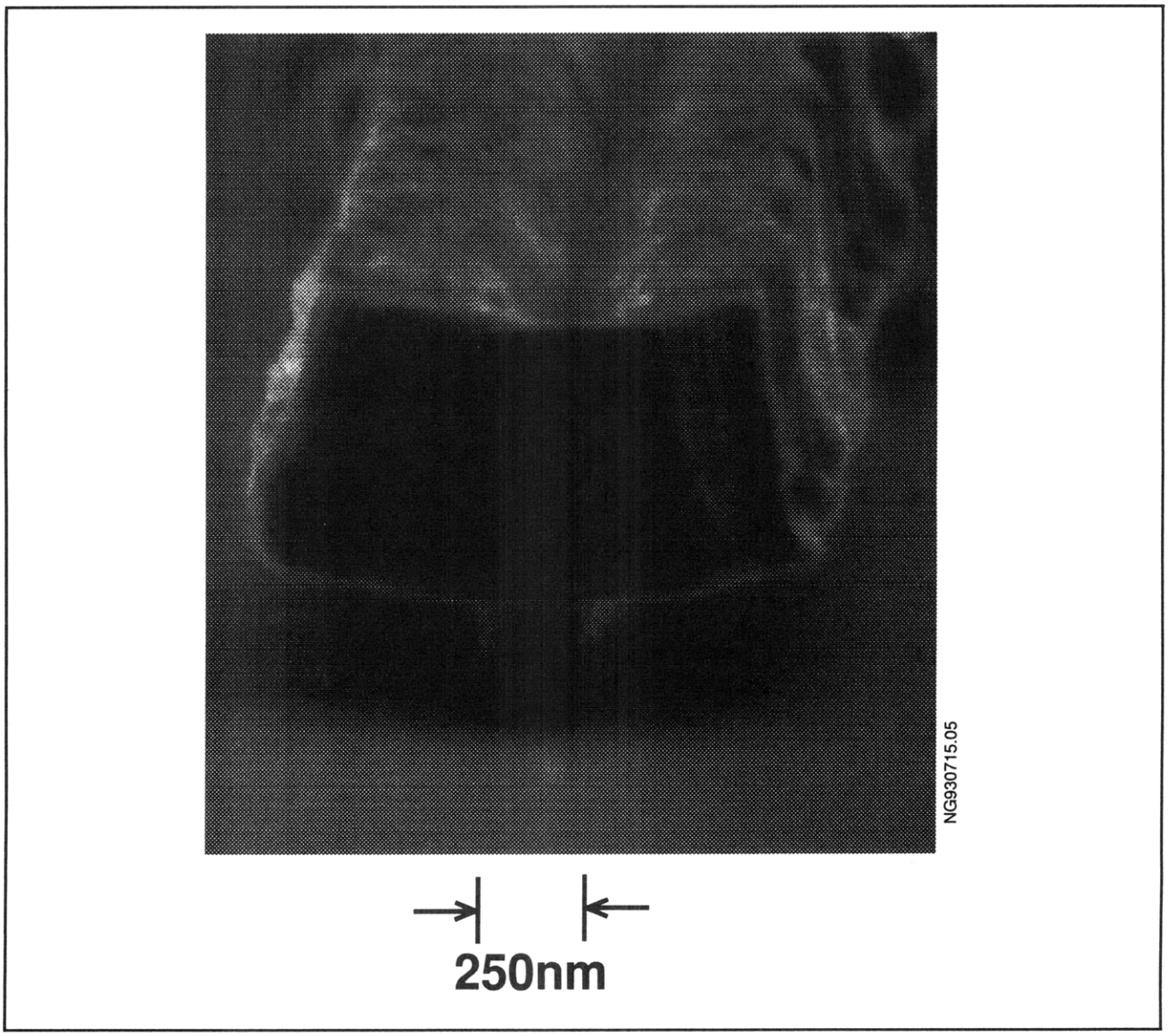

Figure 18. Scanning electron micrograph of a 250 nm T-gate (Ti/Au) after lift-off.

4.12 Studies of Coulomb Charging Effects and Tunneling in Semiconductor Nanostructures

Sponsors

Joint Services Electronics Program
Contract DAAL03-92-C-0001
U.S. Air Force - Office of Scientific Research
Grant F-49-62-92-J-0064

Project Staff

Professor Dimitri A. Antoniadis, Martin Burkhardt, David J. Carter, Arvind Kumar, Professor Michael R. Melloch,[3] Professor Terry P. Orlando, Professor Henry I. Smith

Quantum-effect devices, whose minimum feature sizes are comparable to the Fermi wavelength (about 50 nm in a typical inversion layer), have promising potential in novel electronics applications. Quantum-dot devices have drawn particular attention. In such devices an electron gas is confined electrostatically in all three dimensions, forming a

[3] Purdue University, West Lafayette, Indiana.

small "island" of electrons ~100 nm, bounded on all sides by potential walls. This small electron "island" resembles an atom in that there can be only an integer number of electrons, and these electrons can occupy only certain discrete energy levels. The conductance of the dot, when connected to leads through tunneling barriers, exhibits strong oscillations as the voltage of the gate is varied. Each successive conductance maximum corresponds to the discrete addition of a single electron to the dot. At temperature in the mK range, the conductance decreases by orders of magnitude in between adjacent conductance maxima because there is a large energy cost for an electron in the lead to enter the dot. This energy cost can be removed by changing the gate voltage, resulting in the observed periodic dependence of the conductance on gate voltage.

A variety of tunneling devices were fabricated using x-ray nanolithography and measured at cryogenic temperatures. The devices were fabricated on modulation doped AlGaAs/GaAs substrates. After mesa etch and deposition of ohmic contacts, x-ray nanolithography was used to put down the gate patterns. A typical fabrication sequence for the gate level of a device design is shown in figure 19. After the fabrication of the mother mask using e-beam lithography and electroplating, a daughter mask is made using x-ray lithography at a gap between mother and daughter mask of about 1.5 μm (figure 19b). As an x-ray source we use an electron bombarded copper target emitting Cu_L x-rays (λ = 1.3 nm). The daughter mask is then used to expose device patterns on appropriate semiconductor substrates, as illustrated. For the gates, aluminum was evaporated to a thickness of 120 nm and lifted off. The ability of x-ray lithography to expose vertical profiles in thick resists ensures easy liftoff and simplifies device processing because only one gate metalization is needed.

A novel type of quantum dot device, featuring control over the shape of the quantum dot, was also fabricated using x-ray nanolithography. The device consists of four consecutive quantum point contacts which can be controlled independently. A quantum dot is produced by biasing two pairs of quantum point contacts below the first subband. This allows only tunneling into the out of the dot to take place. The remaining gates can then be used to sweep the electrochemical potential within the dot. The size of the quantum dot can be adjusted up to a size of 600 nm by biasing the two outermost quantum point contacts below the first subband. A micrograph of the fabricated device is shown in figure 20. The device was measured in an Oxford Instruments 300 mK probe. Strong Coulomb blockade oscillations were observed for several Coulomb dot sizes at a temperature of 310 mK. Figure 21 shows a typical plot of conductance versus gate voltage for a quantum dot defined by the two outermost pairs of quantum point contacts.

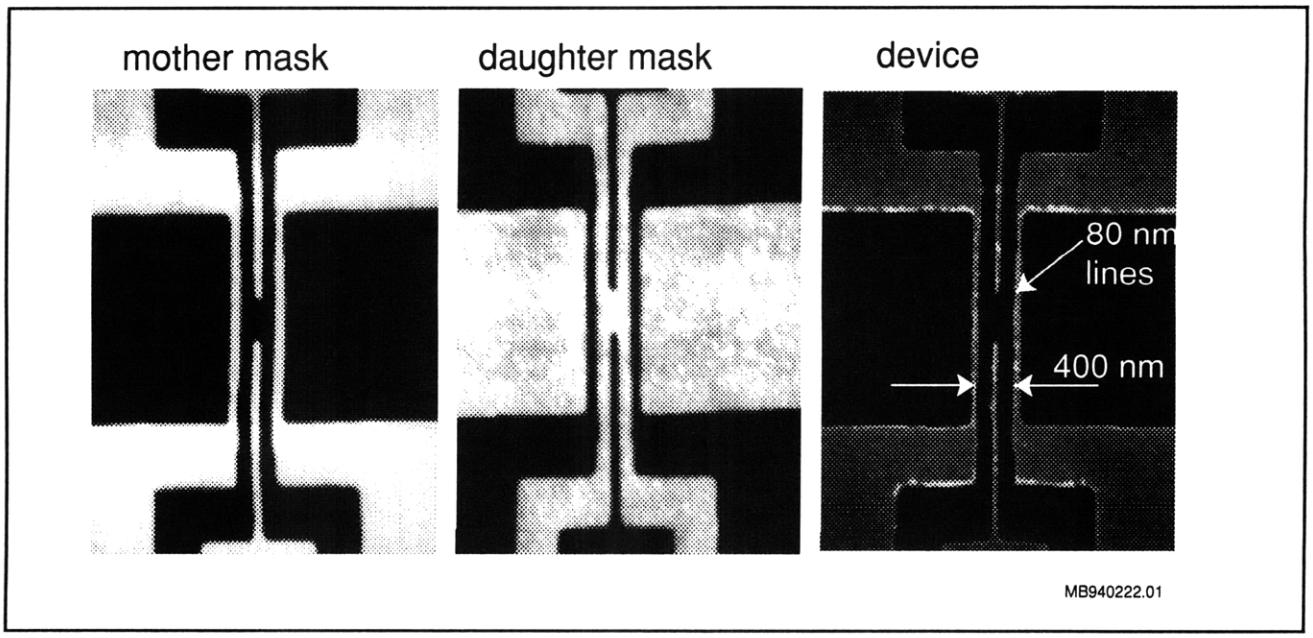

Figure 19. Fabrication sequence of tunnel devices using x-ray nanolithography: (a) mother mask; (b) daughter mask; (c) finished device.

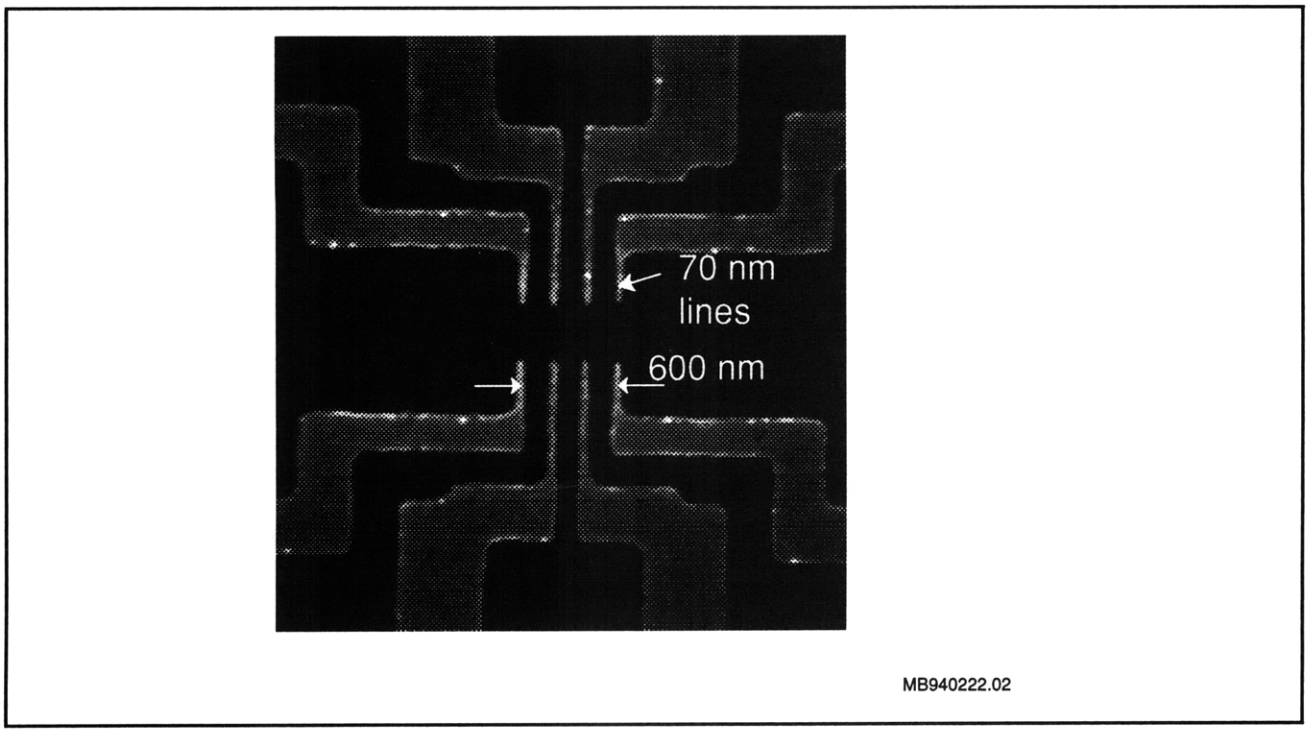

Figure 20. SEM micrograph of the variable sized quantum dot.

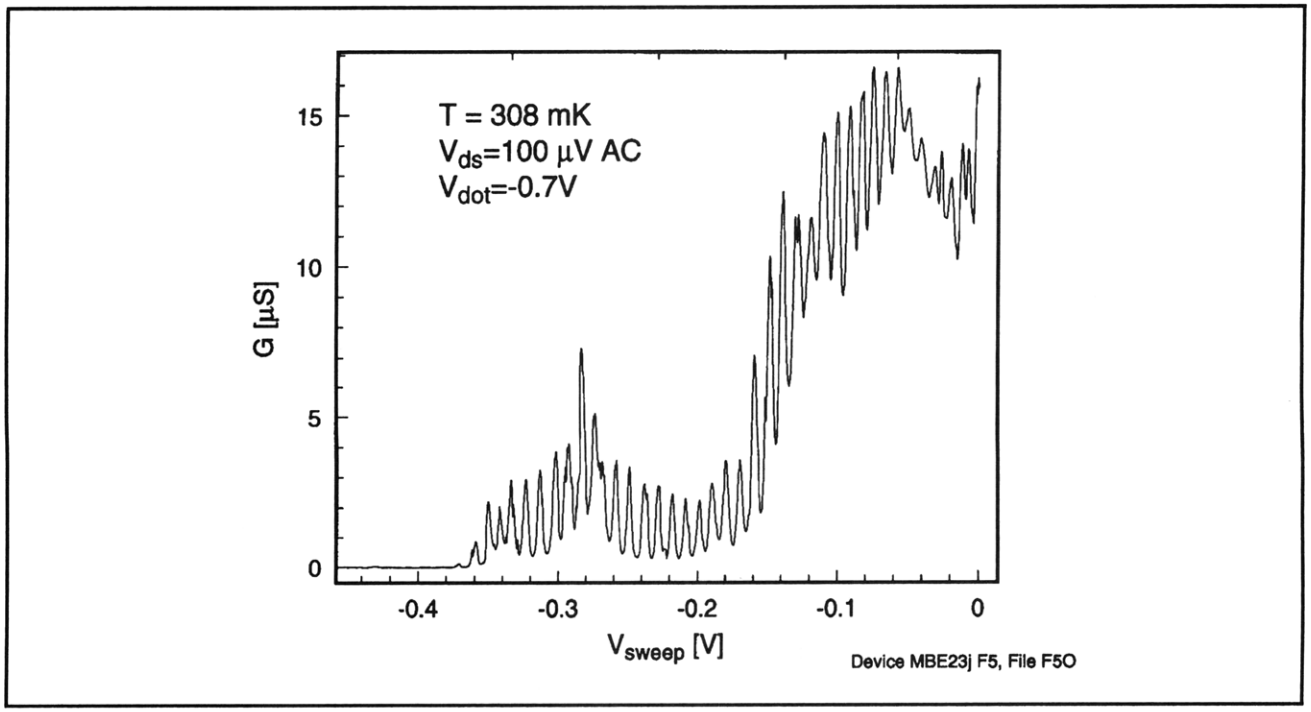

Figure 21. Plot of conductance versus gate voltage for a quantum dot defined by the two outermost pairs of quantum point contacts.

4.13 Dual Electron Waveguide Device Fabricated Using X-ray Lithography

Sponsors

Advanced Research Projects Agency/
Naval Air Systems Command
Contract N00019-92-K-0021
National Science Foundation
Grant DMR 87-19217
Grant DMR 90-22933

Project Staff

Professor Jesús A. del Alamo, William Chu, Christopher C. Eugster, Professor Henry I. Smith

Dual-electron-waveguide devices were fabricated using x-ray nanolithography. An electron waveguide is essentially a one-dimensional channel in which electrons travel without scattering. In our device, two such channels are electrostatically formed in close proximity to one another by depleting those electrons in an AlGaAs/GaAs modulation-doped heterostructure which reside underneath the gates. The x-ray mask used in the fabrication process was patterned using 50 keV e-beam lithography at the Naval Research Laboratory. After replicating this mask to change its polarity (using x-ray lithography), we align the daughter mask to the AlGaAs/GaAs sample and expose using x-ray nanolithography.

In an electron waveguide, much like in an optical waveguide, discrete transverse modes arise due to lateral confinement. The conductance of each waveguide mode is equal to a fundamental constant $2e^2/h$. This results from the cancellation of the energy dependence in the product of the 1D density of states and the electron velocity. Figures 22 and 23 show the results of testing the dual electron waveguides at 1.6K.

4.14 Novel Mesoscopic Superconducting Devices

Sponsor

Joint Services Electronics Program
Contract DAAL03-92-C-0001

Project Staff

Professor Dimitri A. Antoniadis, David J. Carter, James J. Hugunin, Professor Terry P. Orlando, Professor Henry I. Smith

Superconducting integrated circuits have demonstrated fast switching speeds, low power dissipation, and low-loss wiring to distant devices. One of the hurdles between these devices and a practical technology is the lack of a useful three-terminal device. We are currently addressing that problem with the examination of several forms of superconducting FETs on both Si/SiO_2 and GaAs/AlGaAs. By exploiting the quantum interference effects found in very short channel devices (<100 nm), we believe it will be possible to produce three-terminal superconducting devices with gains greater than unity.

In addition to the promise of a practical technology, these devices can be used to investigate several interesting questions in mesoscopic physics. In particular, we are interested in the interaction between the macroscopic quantum states in the superconductor and the mesoscopic quantum states available in traditional quantum-effect devices. By exploiting our experience with quantum dots and quantum point contacts on both Si/SiO_2 and GaAs/AlGaAs, we hope to study the unique effects predicted for these structures with superconducting contacts. These include quantization of the superconducting critical current, supercurrent carried by resonance states, and others.

4.15 Channel-Dropping Filters Fabricated Using X-ray Lithography

Sponsors

Joint Services Electronics Program
Contract DAAL03-92-C-0001
U.S. Army Research Office
Grant DAAL93-92-G-0291

Project Staff

James M. Carter, Jay N. Damask, Juan Ferrera, Professor Hermann A. Haus, Professor Leslie A. Kolodziejski, Euclid E. Moon, Professor Henry I. Smith, Vincent V. Wong

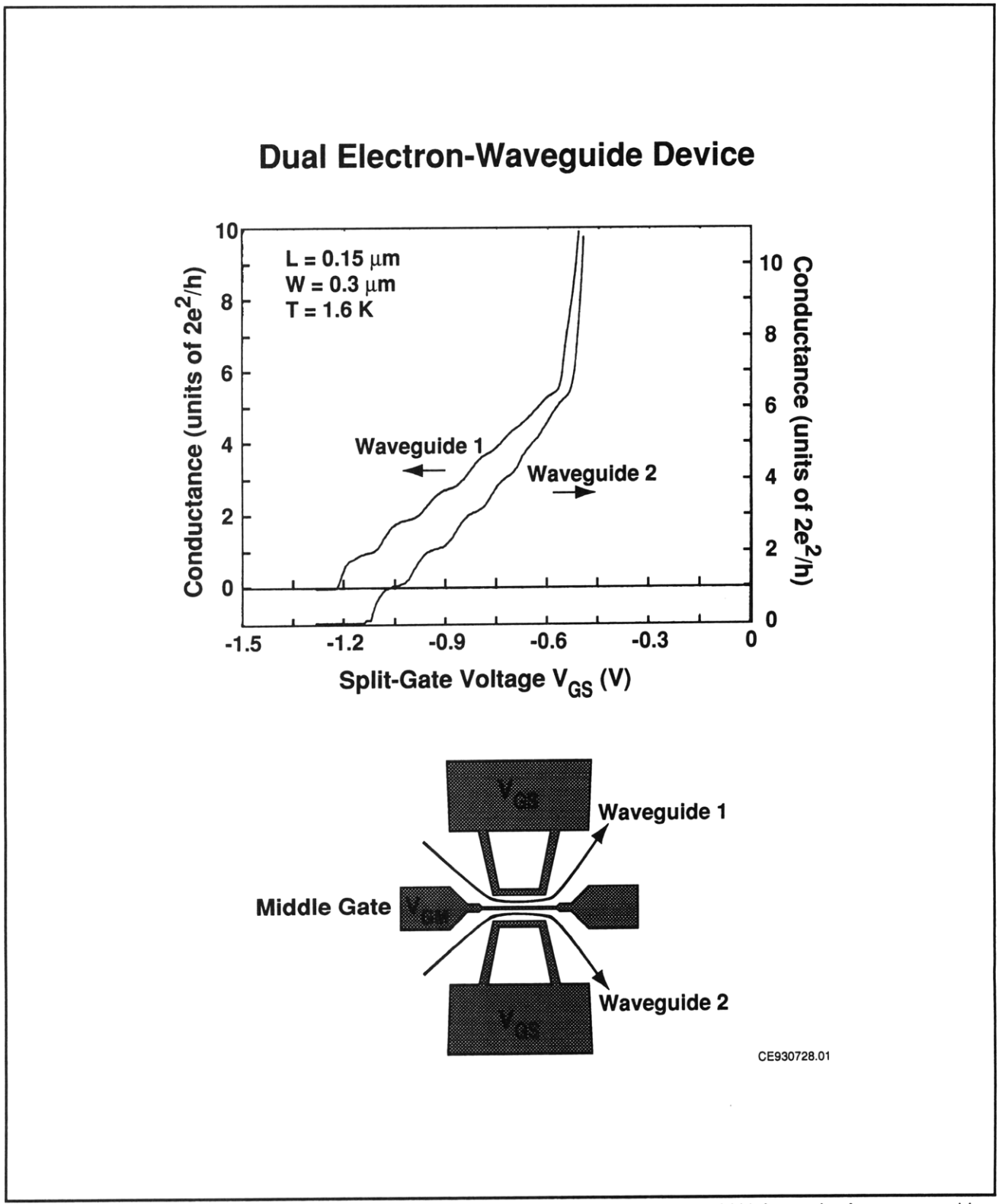

Figure 22. Plot of conductance versus split-gate voltage (proportional to waveguide width) for each of two waveguides, as illustrated. Note that conductance is approximately quantized in steps of $2e^2/h$.

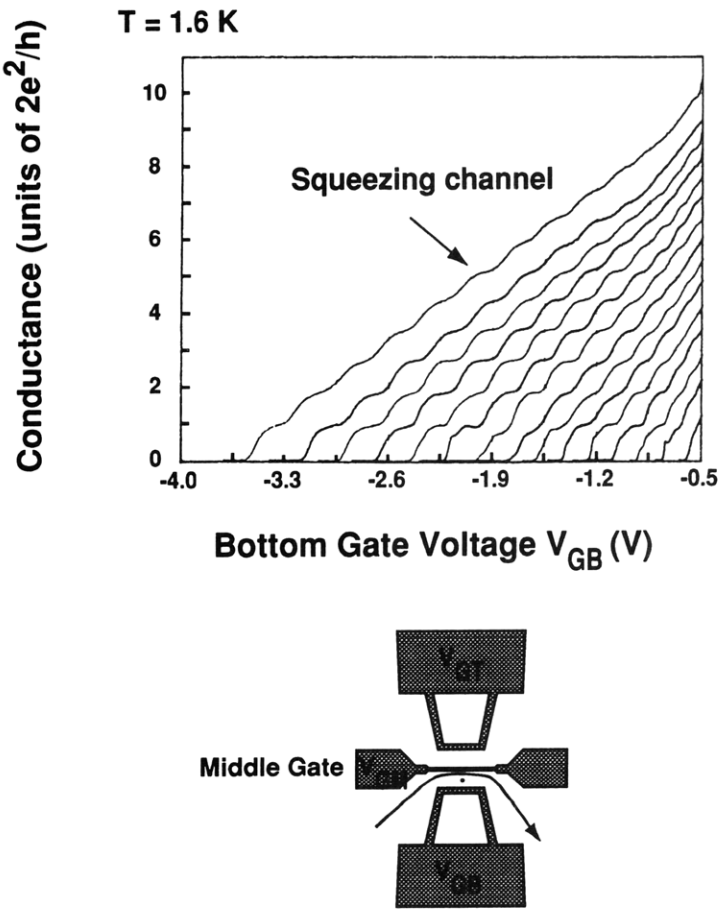

Figure 23. Plot of conductance versus bottom gate voltage for several values of the middle gate bias, which has the effect of shifting the location of the conducting channel. Perturbations of the conductance steps reveal the location of an inpurity in the gap between gates.

Channel-dropping filters (CDFs) are novel optoelectronic devices which are promising candidates for future wavelength-division-multiplexed optical communication systems. Figure 24 shows a schematic of a CDF. The device operation relies on the frequency-selective nature of the quarterwave-shifted (QWS) grating structure, commonly used to improve longitudinal mode control in distributed feedback (DFB) lasers. Such QWS-DFB structures can interact with optical signals in such a way as to selectively transmit, reflect or detect the signals (i.e., wavelengths) that are resonant with the structure. We work with two material systems for the optical waveguides: InGaAsP/InP and silica-on-silicon. For such material systems the necessary grating lengths can span over 1 mm and the grating periods are ~240 nm and ~500 nm for InGaAsP/InP and silica-on-silicon, respectively. Furthermore, the grating lines must be spatially-coherent to within $\lambda_o/150$ over the entire span to reduce linewidth broadening and spectral offsets from the desired resonance, and to avoid spurious responses in the filter spectrum. Recently, we have developed a new technique called spatial-phase-locked e-beam lithography (SPLEBL) which has demonstrated an interfield phase-locking precision standard deviation of σ = 0.35 nm. Figure 4 of section 4.3 shows an e-beam-written QWS-DFB grating with a period of Λ_g = 230 nm. The continuity of the moiré pattern across the field boundaries indicates no discernible stitching error, while the π-phase shift at the QWS boundary (field 3) indicates a true $\lambda/4$ phase step. Using SPLEBL x-ray masks have been written with several QWS-DFB gratings of various lengths and periods.

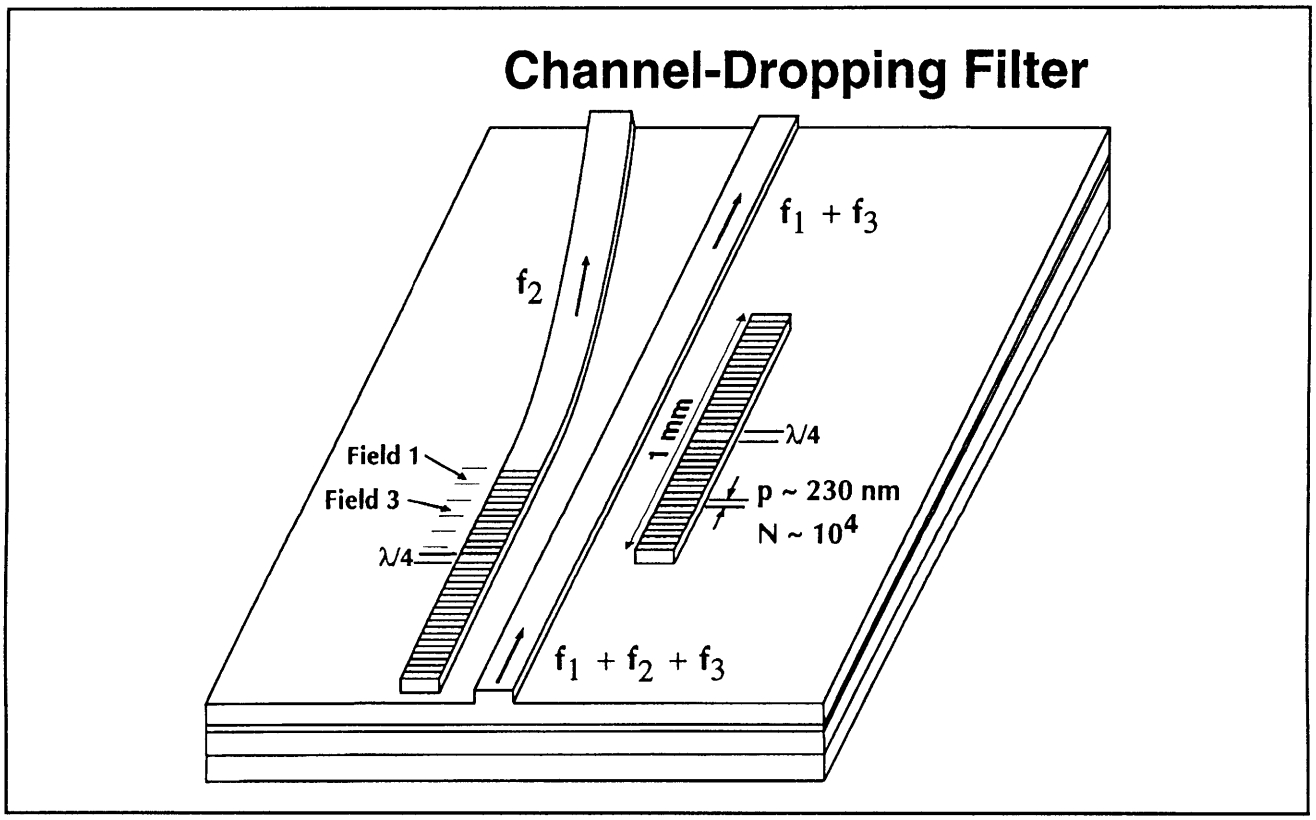

Figure 24. Schematic of a quarter-wave-shifted channel-dropping filter. The gratings, which span several fields of an e-beam lithography system, must be precisely tuned and spatially coherent in order to selectively tap off the narrow channel f_2.

We are also utilizing a novel on-axis interferometric alignment scheme to obtain sub-0.1 μm alignment of the QWS-DFB grating (x-ray level) to the rib waveguides (optical level). Such accuracy is necessary to minimize the resonant effect of the QWS-DFB grating on the unloaded waveguide, or optical bus. X-ray lithography and reactive-ion-etching in CHF_3 is then used to transfer the QWS-DFB gratings into the rib waveguide.

4.16 Ridge-Grating Distributed-Feedback Lasers Fabricated by X-ray Lithography

Sponsors

Joint Services Electronics Program
Contract DAAL03-92-C-0001
U.S. Army Research Office
Grant DAAL03-92-G-0291

Project Staff

James M. Carter, Woo-Young Choi, Juan Ferrera, Professor Clifton G. Fonstad, Jr., Professor Henry I. Smith, Vincent V. Wong

Distributed-feedback lasers are essential components in optical communications systems because they operate in a single-longitudinal-mode and are easily integrable with electronic drive circuitry. In the fabrication of a typical DFB laser, an epitaxial regrowth step is carried out on top of the grating, which can be yield-limiting. In particular, because of etch back the coupling constant after epi-growth can be difficult to predict. We are developing a novel DFB laser structure in which gratings are etched on either side of a ridge waveguide, as shown in figure 25. This structure eliminates the need for regrowth and maximizes the utility of ridge-waveguide devices, which are relatively simple to fabricate. The structure also decouples materials growth, waveguide fabrication and grating fabrication, which should increase device yield.

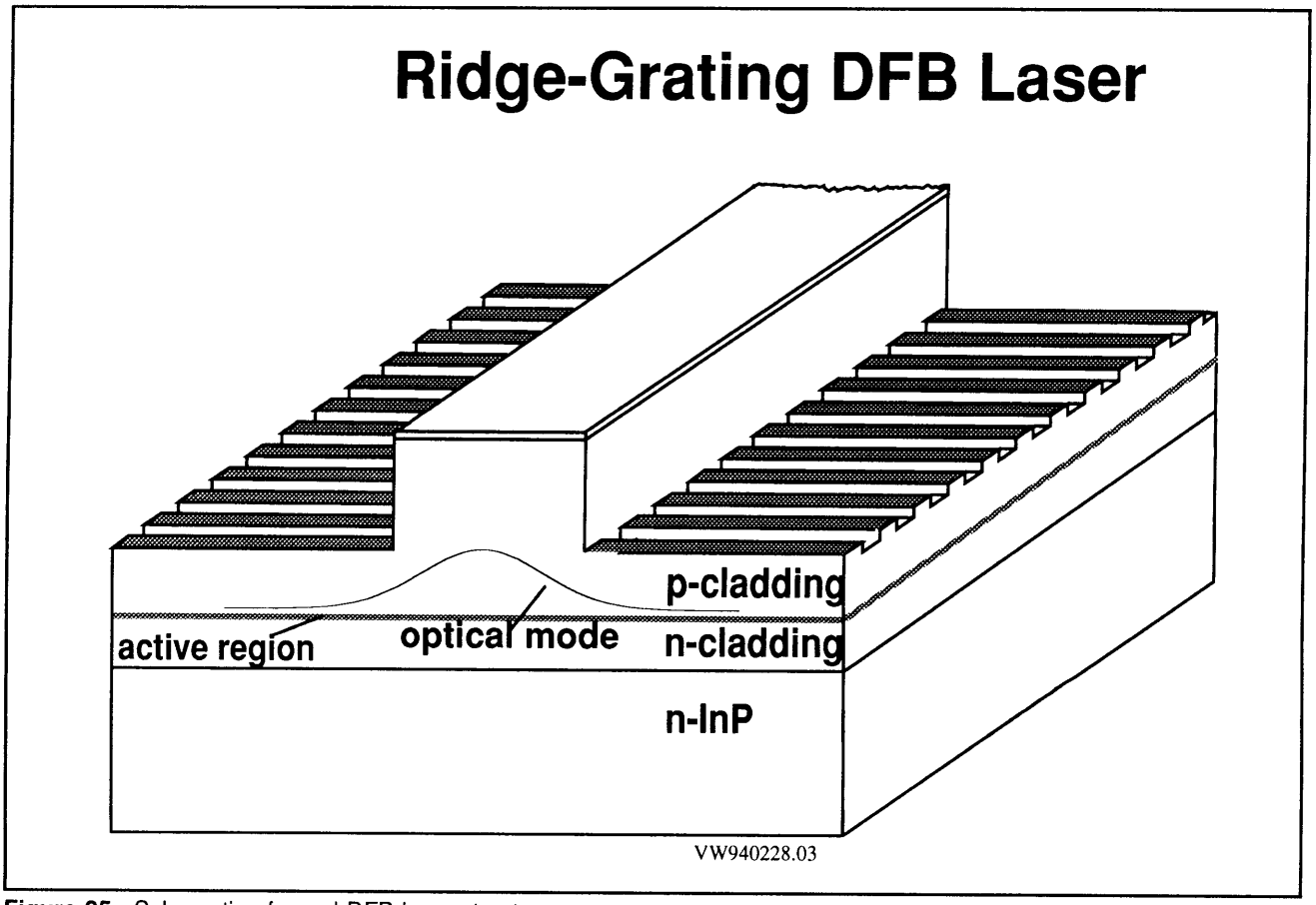

Figure 25. Schematic of novel DFB laser structure.

To realize such a device structure, we have developed a fabrication process that utilizes x-ray lithography for the grating fabrication because it offers good process latitude, high throughput, long-range spatial-phase fidelity in the gratings, and large depth-of-focus. After the epitaxial growth of a complete InGaAlAs graded-index, separate-confinement, multi-quantum-well-layer diode structure, by molecular-beam epitaxy on an InP substrate, a 3-4 μm-wide ridge waveguide is formed by CH_4/H_2 reactive-ion-etching (RIE). A first-order grating with a period of 230 nm for the target lasing wavelength of 1.55 μm is then patterned in PMMA using x-ray nanolithography, as shown in figure 26. The x-ray mask is patterned using holographic lithography, which guarantees excellent uniformity and long-

range spatial-phase coherence in the grating, followed by gold electroplating.

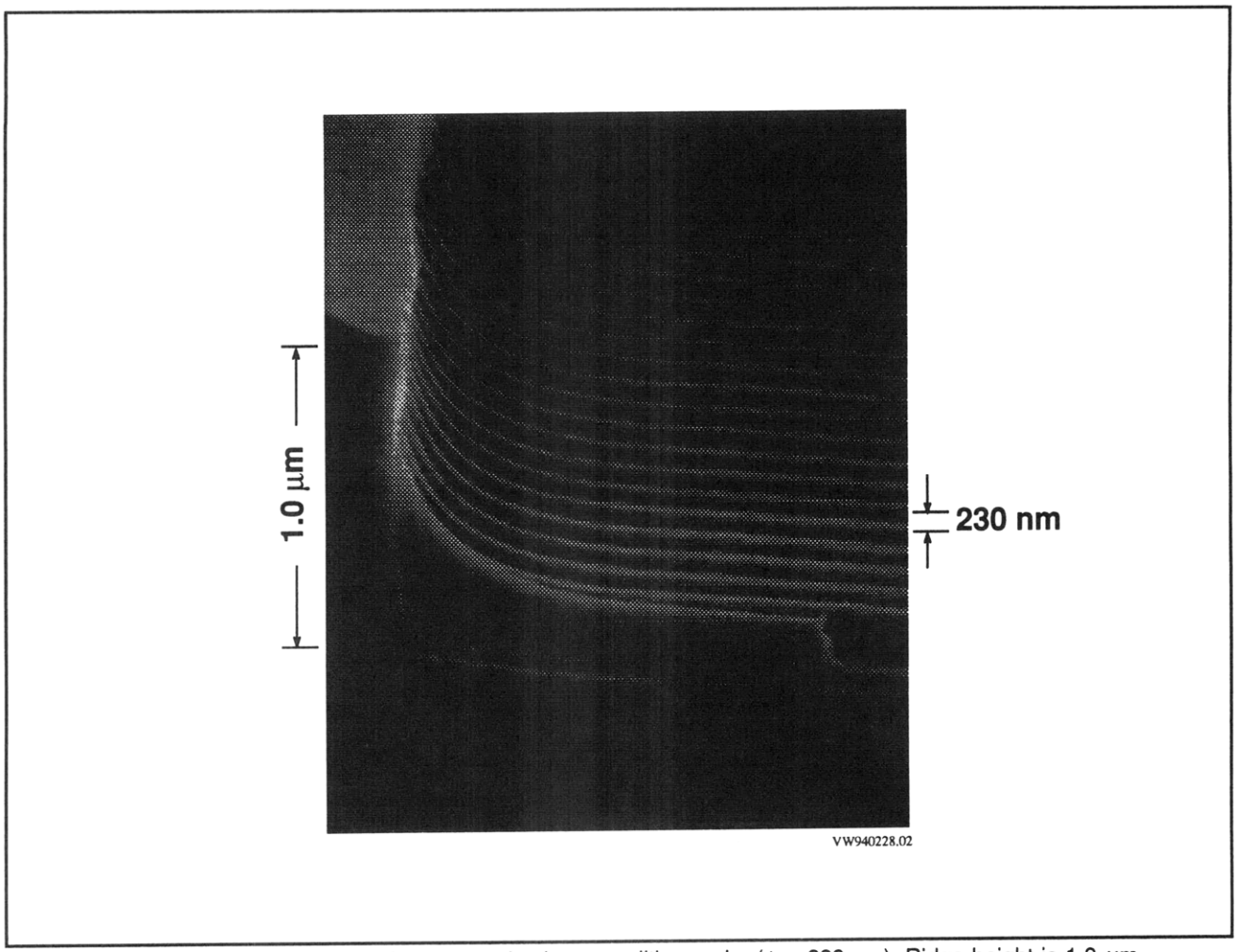

Figure 26. Pattern for DFB laser grating exposed using x-ray lithography (Λ = 230 nm). Ridge height is 1.0 μm.

Reactive-ion etching (RIE) in CHF_3 is used to transfer the grating pattern from PMMA into an oxide hard mask, and subsequent RIE in CH_4/H_2 is used to transfer the grating into both sides of the ridge waveguide. Figure 27 shows an etched InP grating of 250 nm depth next to a ridge waveguide of 1 μm height. As shown, the etched gratings are immediately adjacent to the ridge sidewall, which maximizes the coupling. Figure 3b shows the same InP grating in cross-section. Optical feedback occurs via interaction of the lateral fields with the grating. Holographic lithography could not be used directly for the grating exposure because of troublesome coherent reflections from the ridge topography.

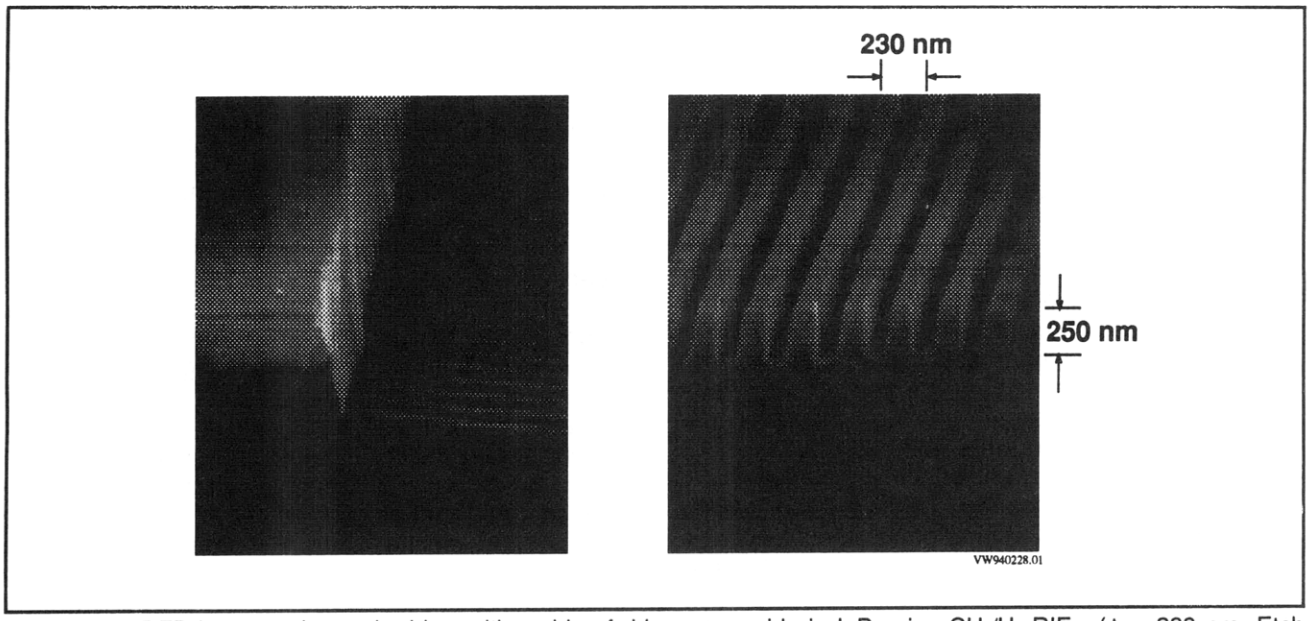

Figure 27. DFB laser grating etched into either side of ridge waveguide in InP using CH_4/H_2 RIE. (Λ = 230 nm. Etch depth = 250 nm).

For advanced optical communication systems (e.g., those implementing wavelength-division multiplexing) quarter-wave-shifted DFB lasers, hundreds of microns in length, are necessary. This will require x-ray masks made by e-beam lithography that are free of distortion and stitching errors. As described in section 4.3 we are pursuing a new technique called spatial-phase-locked e-beam lithography that we believe will solve the problems of distortion and stitching errors.

4.17 Fabrication of Sub-micron MSM Photodiodes by X-ray Lithography

Sponsor

Advanced Research Projects Agency/
Naval Air Systems Command
Contract N00019-92-K-0021

Project Staff

Professor Jesús A. del Alamo, Akbar A. Moolji, Professor Henry I. Smith

Over the last few years, planar InGaAs-InP-based metal-semiconductor-metal (MSM) photodetectors have attracted considerable interest. Among other advantages, their ease of fabrication, high speeds and their compatibility with field-effect transistors are key features that make these devices good candidates for long wavelength, integrated optical communication systems.

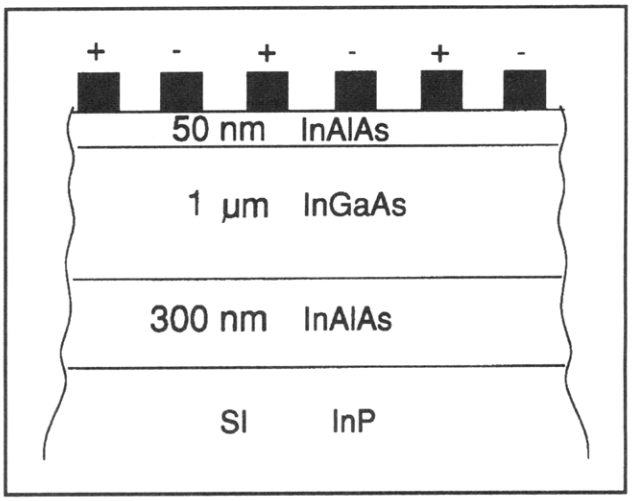

Figure 28. Schematic cross section of a standard MSM photodetector.

Figure 28 is a schematic cross section of the generic MSM photodetector. Work done in the past on these devices has shown this particular combination of layers to be the one that optimizes the operation of the detectors for long wavelengths. The electrode fingers (marked alternately + and –) act as collectors for carriers that are generated when infra-red radiation impinges on the active areas between them. The barrier enhancement layer (50 nm InAlAs), directly below these fingers, serves to enhance the Schottky barrier height of the contact. Since InGaAs itself fails to form a good Schottky contact, the insertion of this thin, high bandgap layer is a necessity that helps suppress the deleterious dark current in these devices. The

300 nm InAlAs buffer layer that lies between the active InGaAs and the semi-insulating InP layers, is the most recent addition to the MSM structure. Its presence has been shown to reduce the parasitic capacitance of the structure over the 100 MHz - 1 GHz range, hence improving the RC-limited bandwidth of the device substantially.

The main bottleneck for the detector bandwidth, however, arises from the transit time of the carriers in the region between the electrode fingers. It is natural to expect that this limitation can be overcome by reducing finger spacing. Detectors with finger spacings down to 0.5 μm have already been reported in the literature. Our efforts are now geared towards pushing this limit even further. The current work is an extension of an earlier effort, made about two years ago at MIT, which yielded good working devices with a bandwidth of about 6 GHz. The smallest finger spacing that was achieved then was about 1 μm. Using otherwise the same fabrication process, we will now pattern the fingers by x-ray nanolithography. This will allow us to scale the finger spacings down to almost 50 nm. Furthermore, the broad process latitude that x-ray nanolithography provides should result in a higher yield of good working devices. More importantly, from a long-range perspective, the large depth-of-focus associated with this technology will permit us to simultaneously fabricate sub-micron size gates for FETs that may then be integrated with these detectors.

As long as the device parasitics are not allowed to dominate, and the detectors can operate in the transit-time limited mode, our efforts should result in structures with greatly improved frequency responses.

4.18 Submicrometer-Period Transmission Gratings for X-ray and Atom-Beam Spectroscopy and Interferometry

Sponsor

Joint Services Electronics Program
Contract DAAL03-92-C-0001

Project Staff

James M. Carter, Julie C. Lew, Jeanne M. Porter, Dr. Mark L. Schattenburg, Satyen Shah, Professor Henry I. Smith

Transmission gratings with periods of 100-1000 nm are finding increasing utility in applications such as x-ray, vacuum-ultraviolet, and atom-beam spectroscopy and interferometry. Over 20 laboratories around the world depend on MIT-supplied gratings in their work. For x-ray and VUV spectroscopy, gratings are made of gold and have periods of 100-1000 nm and thicknesses ranging from 100-1000 nm. They are most commonly used for spectroscopy of the x-ray emission from high-temperature plasmas. Transmission gratings are supported on thin (1 mm) polyimide membranes or made self supporting ("free standing") by the addition of crossing struts (mesh). (For short x-ray wavelengths membrane support is desired, while for the long wavelengths a mesh support is preferred in order to increase efficiency.) Fabrication is performed by holographic lithography, reactive-ion etching and electroplating. Progress in this area tends to focus on improving the yield and flexibility of the fabrication procedures.

Another application is the diffraction of neutral atom beams by mesh supported gratings. Lithographic (holographic and UV proximity) and etching procedures have been developed for fabricating free-standing gratings in thin silicon nitride S_iN_x supported in a Si frame. Figure 29 illustrates the configuration and the method employed to verify freedom from distortion.

We have recently established a collaboration with the Max Planck Institute in Goettingen, Germany, where they will utilize our gratings of 200 and 100 nm period (see section 4.8) in diffraction and interferometer experiments using He atom beams. In addition, free-standing zone plates for use in atom focusing experiments will also be fabricated in S_iN_x.

4.19 High-Dispersion, High Efficiency Transmission Gratings for Astrophysical X-ray Spectroscopy

Sponsor

National Aeronautics and Space Administration
Contract NAS8-36748

Project Staff

Richard J. Aucoin, Professor Claude R. Canizares, Robert C. Fleming, Jeanne Porter, Dr. Mark L. Schattenburg, Professor Henry I. Smith

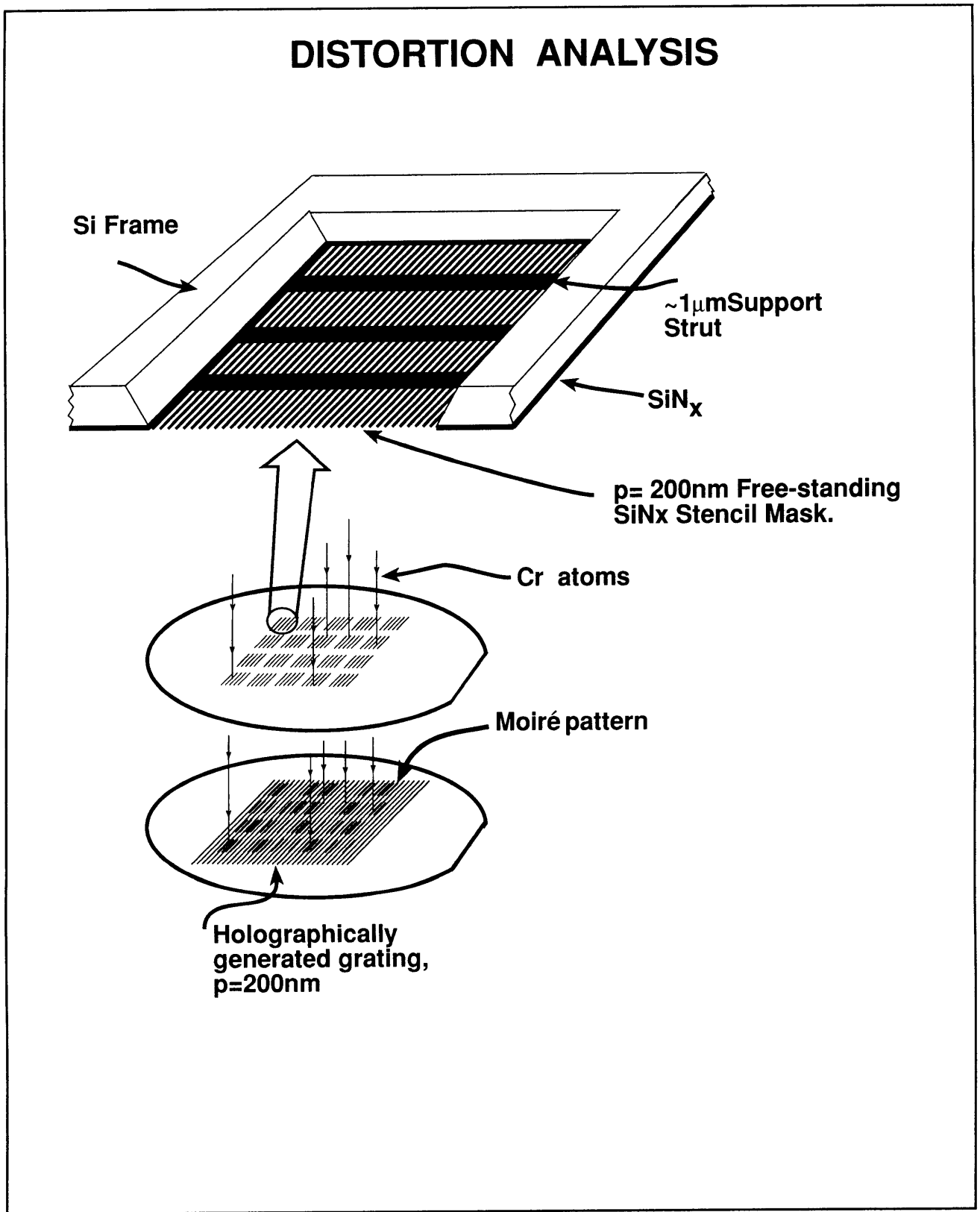

Figure 29. Schematic of the free-standing S_iN_x gratings of 200 nm period. In order to verify that these gratings are free of distortion, chromium atoms were evaporated through the free-standing grating onto a holographically exposed grating of the same period. The resulting moiré fringes reveal the absence of any systematic distortion.

Through a collaboration between the Center for Space Research and the NanoStructures Laboratory (NSL), transmission gratings are provided for the Advanced X-ray Astrophysics Facility (AXAF) x-ray telescope, currently scheduled for launch in 1998. Many hundreds of low-distortion, large-area, gold transmission gratings of 200 nm period and 400 nm period are required. These will provide high resolution x-ray spectroscopy of astrophysical sources in the 100 eV to 10 keV band.

Because of the requirements of low distortion, high yield, and manufacturability, a fabrication procedure involving holographic lithography has been selected. In order to ensure spatial-period fidelity, master reference gratings are used to periodically recalibrate the holography system. The grating patterns are transferred into the substrate using a tri-level resist scheme and reactive-ion etching, followed by gold electroplating. An etching step then yields membrane-supported gratings suitable for space use. Flight prototype gratings have been fabricated and continue to undergo space-worthiness tests. Progress in this area focuses on increasing the yield and flexibility of the fabrication procedures and perfection of grating evaluation tests.

4.20 GaAs Epitaxy on Sawtooth-Patterned Silicon

Sponsor

Joint Services Electronics Program
Contract DAAL03-92-C-0001

Project Staff

Sean M. Donovan, Professor Khalid Ismail,[4] Professor Leslie Kolodziejski, Professor Henry I. Smith, Professor Carl V. Thompson

The growth of GaAs on Si offers the possibility of combining high-speed and optoelectronic GaAs devices with Si integrated-circuit technology. Ordinarily, the 4.1 percent mismatch between the two materials leads to high dislocation densities. However, it has been shown here that when GaAs is grown on sawtooth-patterned Si substrates, the dislocation density is less than $10^5/cm^2$, orders of magnitude lower than in GaAs films grown on planar Si substrates. We investigate this effect both for its potential of greatly improving the quality of GaAs on Si and as a model for understanding the mechanism of dislocation reduction. Oriented gratings of 200 nm period are fabricated in Si_3N_4 on (100) Si substrates using holographic lithography. Anistrotropic etching in KOH is then used to produce sawtooth-profile gratings in the Si. Then these serve as substrates for GaAs growth by gas source MBE.

4.21 Publications

Journal Articles

Burkhardt, M., H.I. Smith, D.A. Antoniadis, T.P. Orlando, M.R. Melloch, K.W. Rhee, and M.C. Peckerar. "Fabrication Using X-ray and Measurement of Coulomb Blockade in a Variable-Sized Quantum Dot." Submitted to *J. Vac. Sci. Technol. B.*

Ferrera, J., V.V. Wong, S. Rishton, V. Boegli, E.H. Anderson, D.P. Kern, and H.I. Smith. "Spatial-Phase-Locked Electron-Beam Lithography: Initial Test Results." *J. Vac. Sci. Technol. B* 11: 2342-2345 (1993).

Gupta, N., S.D. Hector, K.W. Rhee, and H.I. Smith. "Fabrication of 100 nm T-Gates for Monolithic Microwave Integrated Circuits Using X-ray Lithography." *J. Vac. Sci. Technol. B* 11: 2625-2628 (1993).

Hector, S.D., H.I. Smith, and M.L. Schattenburg. "Simultaneous Optimization of Spectrum, Spatial Coherence, Gap, Feature Bias, and Absorber Thickness in Synchrotron-Based X-ray Lithography." *J. Vac. Sci. Technol. B* 11: 2981-2985 (1993).

Hector, S.D., V.V. Wong, H.I. Smith, M.A. McCord, A. Wagner, and K.W. Rhee. "Optimizing Exposure Latitude as a Function of Absorber Thickness and Gap in X-ray Lithography." Submitted to *J. Vac. Sci. Technol. B.*

Hu, H., I.Y. Yang, L.T. Su, V.V. Wong, M. Burkhardt, E. Moon, J. Carter, D.A. Antoniadis, H.I. Smith, K.W. Rhee, and W. Chu. "High Performance Self-Aligned Sub-100 nm MOSFETs using X-ray Lithography." Submitted to *J. Vac. Sci. Technol. B.*

Li, H., M. Mondol, G. Owen, and H.I. Smith. "Uniform, Zero-Stress W via He-Backside Tem-

[4] Cairo University.

perature Stabilization." Submitted to *J. Vac. Sci. Technol. B.*

Moel, A., E.E. Moon, R. Frankel, and H.I. Smith. "Novel On-axis Interferometric Alignment Method with Sub-10 nm Precision." *J. Vac. Sci. Technol. B* 11: 2191-2194 (1993).

Schattenburg, M.L., N.A. Polce, and H.I. Smith. "Fabrication of Flip-Bonded Mesa Masks for X-ray Lithography." *J. Vac. Sci. Technol. B* 11: 2906-2909 (1993).

Smith, H.I., and M.L. Schattenburg. "X-ray Lithography, from 500 to 30 nm: X-ray Nanolithography." *IBM J. Res. Dev.* 37: 319-329 (1993).

Wong, V.V., W.-Y. Choi, J. Carter, C.G. Fonstad, and H.I. Smith. "Ridge-Waveguide Sidewall-Grating Distributed Feedback Structures Fabricated by X-ray Lithography." *J. Vac. Sci. Technol. B* 11: 2621-2624 (1993).

Wong, V.V., J. Ferrera, J. Damask, J. Carter, E. Moon, H.A. Haus, H.I. Smith, and S. Rishton. "Channel-Dropping Filters on $SiO_2/Si_3N_4/Si$ Fabricated using X-ray Lithography." Submitted to *J. Vac. Sci. Technol. B.*

Yanof, A.W., G.L. Zipfel, and E.E. Moon. "X-ray Mask Membrane Motion in Narrow Gap Lithography: Hydrodynamic Model and Experiment." *J. Vac. Sci. Technol. B* 11: 2920-2925 (1993).

Zhao, Y., D.C. Tsui, M. Santos, M. Shayegan, R.A. Ghanbari, D.A. Antoniadis, H.I. Smith, and K. Kempa. "Mode Softening in the Far Infrared Excitation of Quantum Wire Arrays." *Phys. Rev. B* 48: 5249-5255 (1993).

Meeting Papers

Bozler, C.O., C.T. Harris, S. Rabe, D.D. Rathman, W.D. Goodhue, M.A. Hollis, and H.I. Smith. "Arrays of Gated Field-Emitter Cones having 0.32 μm Tip-to-Tip Spacings." Paper presented at the Sixth International Vacuum Microelectronics Conference, Newport, Rhode Island, July 12-15, 1993.

Bozler, C.O., C.T. Harris, S. Rabe, D.D. Rathman, W.D. Goodhue, M.A. Hollis, and H.I. Smith. "Fabrication and Performance of Gated Field-Emitter Arrays Having 0.32 μm Tip-to-Tip Spacings." Paper presented at the Electrochemical Society Meeting, New Orleans, Louisiana, October 10-15, 1993.

Choi, W.Y., V.V. Wong, J.C. Chen, H.I. Smith, and C.G. Fonstad. "Design and Fabrication using X-Ray Lithography of Ridge-Waveguide Distributed Feedback Structures on InP." Paper presented at the International Conference on InP and Related Compounds, Santa Barbara, California, March 1994.

Damask, J.N., V.V. Wong, J. Ferrera, H.I. Smith, and H.A. Haus. "Optical Distributed-Feedback Channel-Dropping Filters: Design and Fabrication." LEOS '93 Sixth Annual Meeting, San Jose, California, November 15-18, 1993 (Invited Paper).

Damask, J.N., J. Ferrera, V.V. Wong, H.I. Smith, L.A. Kolodziejski, and H.A. Haus. "Limitations and Solutions for the Use of Integrated QWS-DBR Resonators in WDM Applications." Paper presented at the International Symposium on Integrated Optics '94, Lindau, Germany, April 11-15, 1994.

Ferrera, J., J.N. Damask, V.V. Wong, H.I. Smith, and H.A. Haus. "High-Coherence QWS Gratings for Optoelectronic Devices: Why Spatial-Phase-Locked E-Beam Lithography is Necessary." Paper to be presented at the Fiber Communications Conference '94, San Jose, California, February 20-25, 1994.

Ferrera, J., J.N. Damask, V.V. Wong, H.I. Smith, and H.A. Haus. "High-Coherence QWS Gratings for Optoelectronic Devices: Why Spatial-Phase-Locked E-Beam Lithography is Necessary." Paper submitted to the Optical Fiber Communications Conference '94, San Jose, California, September 11, 1993.

Hector S.D., and H.I. Smith. "Soft X-ray Projection Lithography Using Two Arrays of Phase Zone Plates." In *Proceedings of The Optical Society of America Meeting on Soft X-ray Projection Lithography* 18, 202-206. Eds. A.M. Hawryluk and R.H. Stulen. Washington, D.C.: Optical Society of America, 1993.

Hector, S.D., H.I. Smith, N. Gupta, and M.L. Schattenburg. "Optimizing Synchrotron-Based X-ray Lithography for 0.1 μm Lithography." Paper presented at the Microcircuit Engineering '93 Meeting, Maastricht, The Netherlands, September 27-29, 1993. Microelectron. Eng. 23: 203-206 (1994).

Hu, H., L.T. Su, I.Y. Yang, D.A. Antoniadis, and H.I. Smith. "Channel and Source/Drain Engineering in High-Performance Sub-0.1 μm NMOSFETs Using X-ray Lithography." Paper to be presented

at the Symposium on VLSI Technology, Honolulu, Hawaii, June 7-9, 1994.

Schattenburg, M.L., J. Carter, W. Chu, R.C. Fleming, R.A. Ghanbari, M. Mondol, N. Polce, and H.I. Smith. "Mask Technology for X-ray Nanolithography." *Proceedings of the Material Research Society Symposium* 306: 63-68 (1993).

Smith, H.I., and M.L. Schattenburg. "X-ray Nanolithography: Limits, and Application to Sub-100 nm Manufacturing." Paper presented at the NATO Workshop on Nanolithography, Rome, Italy April 6-8, 1993.

Zhao, Y., D.C. Tsui, M.B. Santos, M. Shayegan, R.A. Ghanbari, D.A. Antoniadis, H.I. Smith, and K. Kempa. "Mode Softening of Coupled Quantum Wires." Paper submitted to the Tenth International Conference on the Electronic Properties of Two-Dimensional Systems, Salva Regina University, Newport, Rhode Island, May 31-June 4, 1993.

Theses

Chu, W. *Inorganic X-ray Mask Technology for Quantum-Effect Devices.* Ph.D. diss., Dept. of Electr. Eng. and Comput. Sci., MIT, 1993.

Damask, J.N. *A New Photonic Device: The Integrated Resonant Channel-Dropping Filter.* M.S. thesis, Dept. of Electr. Eng. and Comput. Sci., MIT, 1993.

Ghanbari, R.A. *Physics and Fabrication of Quasi-One-Dimensional Conductors.* Ph.D. diss., Dept. of Electr. Eng. and Comput. Sci., MIT, 1993.

Gupta, N. *Fabrication of 100 nm T-Gates for Monolithic Microwave Integrated Circuits using X-ray Lithography.* S.M. thesis, Dept. of Electr. Eng. and Comput. Sci., MIT, 1993.

Lew, J.C. *Fabrication of Free-Standing Silicon Nitride Gratings of 200 nm Period for Atom Interferometry.* S.B. thesis, Dept. of Electr. Eng. and Comput. Sci., MIT, 1993.

Lim, M.H. *Measurement of In-Plane Distortion using Holographic Interferometric Techniques.* S.B. thesis, Dept. of Electr. Eng. and Comput. Sci., MIT, 1993.

Rittenhouse, G.E. *Mesoscopic Transport of Cooper Pairs through Ballistic Superconductor-Normal Metal-Superconductor Junctions.* Ph.D. diss., Dept. of Electr. Eng. and Comput. Sci., MIT, 1993.

Shah, S.N. *A White Light Interferometer for Improved Achromatic Holographic Lithography.* S.B. thesis, Dept. of Electr. Eng. and Comput. Sci., MIT, 1993.

MIT Patents

Smith, H.I., A.M. Modiano, and E. Moon, "Optical Aligning." Patent application submitted to U.S. Patent Office, 1993.